Glacial - periglacial transition in the Ratera Cirque (Central Pyrenees) from the Younger Dryas to the Holocene

Josep Ventura, Marc Oliva, José Fernández-Fernández, Marcelo Fernandes, David Palacios, Tancrède Leger, Vincent Jomelli, Aster Team

Quaternary Science Advances 20 (2025) 100307

Contents lists available at ScienceDirect

Quaternary Science Advances

journal homepage: www.sciencedirect.com/journal/quaternary-science-advances

Glacial - periglacial transition in the Ratera Cirque (Central Pyrenees) from the Younger Dryas to the Holocene

Josep Ventura [a,*], Marc Oliva [a], José M. Fernández-Fernández [b], Marcelo Fernandes [c], David Palacios [b], Tancrède Leger [d], Vincent Jomelli [e], Aster Team [e]

[a] Department of Geography, Universitat de Barcelona, Montalegre 6, 08001, Barcelona, Catalonia, Spain
[b] Department of Geography, Universidad Complutense de Madrid, Calle del Profesor Aranguren, s/n. Facultad de Geografía e Historia, Ciudad Universitaria, 28040, Madrid, Spain
[c] Centre of Geographical Studies, Institute of Geography and Spatial Planning, Universidade de Lisboa, Rua Branca Edmée Marques, 1600-276, Lisboa, Portugal
[d] Institute of Earth Surface Dynamics, University of Lausanne, Lausanne, Switzerland
[e] CEREGE, UMR 34 Aix-Marseille University-CNRS-IRD-Coll, France-INRAE, 13545 Aix-en-Provence, France

ARTICLE INFO

Keywords:
Deglaciation, Heinrich 1, Bølling-Allerød
Younger dryas
Early holocene
Debris-covered glaciers
Rock glaciers
Paraglacial processes
Cosmic-ray exposure dating
Central pyrenees

ABSTRACT

The transition from glacial to deglacial environments in mid-latitude mountains leaves a wide range of landforms of glacial, periglacial and paraglacial origin, of which the chronology and evolution are still debated. This work provides geomorphological and geochronological evidence for the last phases of deglaciation in the Ratera Valley and cirque (upper Noguera Pallaresa Valley-Central Pyrenees) by applying cosmic-ray exposure (CRE) dating to a set of 19 samples from moraine boulders, rock glaciers and glacially polished surfaces. The results indicate the occurrence of several glacial and periglacial phases between the end of Heinrich 1 (HS-1) event and the Mid-Early Holocene. The deglaciation of the Ratera area occurred between ca. 15.3 and 13.4 ka, interrupted by small glacial advances and/or standstills evidenced by the formation of moraine ridges. The moraine complex closing the Ratera Cirque was formed during the Bølling/Allerød (B-A) – Younger Dryas (YD) transition at ca. 12.6–12.4 ka. Later, during the Early Holocene, this glacier developed into a debris-covered glacier, which stabilised at ca. 9.9 ± 0.9 ka. Subsequently, this debris-covered glacier was partly fossilised by a rock glacier consisting of two differentiated units which stabilised at ca. 8.8 ± 0.8 and 5.8 ± 0.6 ka, respectively. Finally, a small debris-free glacier built a moraine ridge at the foot of the cirque wall. Thus, this spatio-temporal pattern of deglaciation of the Ratera Cirque represents a unique case spanning 10 ka, providing evidence of the major environmental changes that followed the disappearance of glaciers in the Pyrenees and demonstrates the importance of past periglacial and paraglacial dynamics in shaping the present-day mountain landscape in this range.

1. Introduction

While the local maximum ice extent of the Last Glacial Cycle (LGC; 115-14 ka) in the Pyrenees occurred before the global Last Glacial Maximum (LGM; 26-19 ka), during the Marine Isotopic Stage (MIS) 4 (71-57 ka), the evolution of Pyrenean glaciers during the last deglaciation (Termination-1, T-1; 19-11 ka) followed similar spatio-temporal patterns in the Iberian mountains (Oliva et al., 2019; López-Moreno et al., 2018), in sync with the rest of the major European mountain ranges; Alps, Carpathians, Scandinavian Alps, Apennines, etc. (Ivy-Ochs, 2015; Makos, 2015; Palacios et al., 2023).

The climate variability prevailing in the North Atlantic region during T-1 led to widespread glacial advance and retreat within the long-term warming trend (Buizert et al., 2018; Rea et al., 2020).

During T-1, the European glaciers generally advanced during Heinrich 1 (HS-1; ~18–14.6 ka; GS-2; Rasmussen et al., 2014; Naughton et al., 2023a), retreated during the Bølling-Allerød (B-A; 14.6–12.9 ka; GI-1), and expanded again during the Younger Dryas (YD, 12.9–11.7 ka; GS-1). The European glaciers retreated drastically during the Holocene (Walker et al., 2018), with some short and intermittent periods of expansion during the so-called Neoglacial period (since ~4–6 ka; Solomina et al., 2015; García-Ruiz et al., 2020). Indeed, knowledge of glacial

* Corresponding author. author.
E-mail address: jventuraroca2@gmail.com (J. Ventura).

https://doi.org/10.1016/j.qsa.2025.100307
Received 15 September 2025; Received in revised form 25 November 2025; Accepted 27 November 2025
Available online 29 November 2025

stadials of the last few millennia is still very limited (Oliva et al., 2019; Delmas et al., 2023a,b,c, ; Delmas et al., 2024), with the Little Ice Age (LIA; XIV-XIX century) being the best known Late Holocene glacial pulse in the Pyrenees (García-Ruiz et al., 2020) and in southern Europe (Oliva & Gómez-Ortiz, 2012).

Glacial landforms can be dated using various methods, depending on study objectives, sample type, and chronological framework (Davies, 2022). In the Pyrenees, radiocarbon (^{14}C) dating of organic remains in glacial deposits provided the first absolute ages for the Last Glacial Cycle (LGC), reaching up to ~40 ka in the 1980s (Oliva et al., 2019). However, most ^{14}C samples derived from low- and mid-altitude proglacial or juxtaglacial lakes, peat bogs, or cirque floors below 2000 m a.s.l., leaving high mountain environments largely unexplored. In the late 1990s, Optically Stimulated Luminescence (OSL) dating of fluvioglacial sediments extended the chronology of the LGC to ~80–90 ka and enabled the dating of older terraces. More recently, cosmic-ray exposure (CRE) dating, introduced in the Pyrenees in 2006 (Pallàs et al., 2006), has redefined regional glacial chronologies (Delmas et al., 2021). Its growing application in this mountain range has generated a substantial body of chronological data, shedding new light on geomorphological evolution during the final stages of deglaciation and improving earlier chronologies, which were based on very few dates and were particularly scarce for this period (Bordonau et al., 1992; Pallàs et al., 2006).

The most complete glacial–periglacial sequences, in terms of the number, variety, and age of landforms, have been identified in the Piniecho cirques of the Tena Valley (Palacios et al., 2015), the Medacorba area, Soulcem Valley (Jomelli et al., 2020) and Baciver, Aran Valley (Oliva et al., 2021; Fernandes et al., 2023) in the Central Pyrenees.

This study presents new geochronological data to improve the chronology of the last deglaciation of the Pyrenees (T-1 and Holocene) in the Noguera Pallaresa basin (Central southern Pyrenees), the most extensive glacial system on the southern slope of the Pyrenees, but whose deglaciation still lacks robust geochronological data. The objectives of this study are as follows.

- To present new CRE dates for the last glacial oscillations in the Noguera Pallaresa basin.
- To reconstruct the deglacial environmental evolution in the Ratera Cirque and valley based on the geomorphological mapping and CRE dating of a wide range of landforms, such as rock glaciers, moraines, and debris-covered glacier moraines as representative of the transition from glacial to periglacial and paraglacial environments.
- To compare the results from the Ratera Cirque (southern slope) with the geochronological data available for (i) the neighbouring Ruda Valley (northern slope) and with other environmental and climatic studies from the same massif, to better understand the topoclimatic and morphometric controls on postglacial evolution, and (ii) other mountain ranges of the Mediterranean basin.

2. Study area

2.1. General study area background

The Pyrenees constitute a mountain range that separates the Iberian Peninsula from the rest of the European continent, extending W-E for ca. 500 km. The highest elevations (over 3300 m a.s.l.) are found in the Maladeta batholith, in the central Pyrenees, between the Ésera (West) and Noguera Pallaresa valleys (East). The study area is in the western sector of the Ratera Cirque and valley (Tuc de Ratera, 2861 m a.s.l.; 42° 36′ 04″ N, 0° 57′ 11″ E; Fig. 1B), on the NE edge of the Comalesbienes-Colomèrs-Basiero Massif (Punta Alta, 3014 m a.s.l.). The area is drained by the Escrita River (Fig. 1B), a tributary of the Noguera Pallaresa (Fig. 1), and is included in the National Park of Aigüestortes and Estany de Sant Maurici.

The coalescent cirque of Ratera (8.2 km^2) consists of eight individual cirques excavated on the S-SE slopes of the Saboredo (2830 m a.s.l.; Fig. 1B) and Bassiero peaks (2903 m a.s.l.; Fig. 1B). The relatively flat surfaces at the summit correspond to the remnants of ancient preglacial erosion surfaces (Martí-Bono and Puigdefàbregas, 1968; Ventura, 1983) and to diffluence cols between the sharp peaks. The Ratera Cirque was one of the two accumulation areas of the former Escrita Glacier, a tributary of the main Noguera Pallaresa paleoglacier (Ventura and Turu, 2022).

The Maladeta granitic batholith of Carboniferous-Permian age forms part of the Lower Pyrenean Mantos, which contain exclusively Paleozoic lithologies (Muñoz, 1992). The basement consists of biotitic-hornblende granodiorite crossed by a NW-SE oriented dyke of dioritic and quartz-odioritic porphyry following shear bands (Leblanc and Gleizes, 1991; ICGC, 2007). One of these bands crosses the area in a NW-SE direction and controls the inner geomorphological setting of the Ratera Cirque, with the alignment of several overdeepened glacial basins.

The Bonaigua weather station (2266 m a.s.l.), 5.5 km north of the Ratera Cirque, records a mean annual air temperature (MAAT) of 2.8 °C and an average annual precipitation of 1187 mm (period 2007–2016). At 2200–2300 m, the snow cover lasts generally from November to the beginning of June (average thickness of 106 cm over the same period). In the Ratera Cirque, long-lasting snow patches persist in NE-E sheltered areas below the ridges at 2650–2725 m. For the central Pyrda (2023) estimated that the regional 0 °C MAAT isotherm is located at ca. 2950 m a.s.l.

The vegetation at the bottom of the cirque consists of increasingly open subalpine black pine (*Pinus uncinata*) forest combined with alpine meadows (Carrillo and Ninot, 1998). The tree line is at 2450 m a.s.l., and above 2500 m a.s.l., the rocky tundra prevails, with large areas of glacially polished surfaces, ridges and cirque walls, and widespread talus scree.

2.2. Background on the glacial geomorphological setting of the study area

The geomorphology of the headwaters of the Ratera Valley, including the Ratera area (Fig. 1B), has been studied since 1930's, when the main moraines and glacial deposits were identified (Nussbaum, 1934, 1956; García-Sainz, 1935; Solé i Sabarís, 1936). Fontboté et al. (1957) assigned the moraines to younger or older glaciations on the basis of the petrographic characteristics of the deposits, their degree of weathering and their relationship with interglacial deposits (paleosols). The authors established a relative chronology, identifying "external moraines" attributed to the Riss glaciation at 1250 m a.s.l. in the Espot Valley and "internal moraines" of the Würm glaciation at 1900 m a.s.l. near Sant Maurici Lake (Fig. 1B). Taillefer (1957) described the presence of moraine arches with angular blocks in the cirques (referring to rock glaciers, but without naming them as such). Hamelin (1958) described the debris accumulations in the Portarró d'Espot cirque (Fig. 1B) as rock glaciers. Zandvliet (1960) produced a geomorphological map at a scale of 1:100,000, identifying the main glacial features of the Noguera Pallaresa paleoglacier system and several rock glaciers in the cirques. Martí-Bono and Puigdefàbregas (1968) highlighted the tectonic control on the orientation of the Ratera Valley, estimated the Equilibrium Line Altitude (ELA) at 2100–2200 m a.s.l during the maximum ice extent of the LGC and described the relatively flat summits of the area as cryoplanation surfaces. Years later, Ventura (1983) mapped the main glacial erosion and accumulation landforms in the Espot Valley at a scale of 1:25,000, attributing them to the last deglaciation but without absolute chronological control (Bru et al., 1985; Bordonau et al., 1992; Serrat et al., 1994).

Recently, Ventura and Turu (2022) presented a new synthesis of the current knowledge of glacial geomorphology in the central-eastern Pyrenees with the spatial reconstruction of the Noguera Pallaresa paleoglacier. It was the longest glacier flowing on the southern slope of the Pyrenees and originated in the Ratera Cirque. To date, the chronological framework of past glaciations in this valley includes (i) evidence

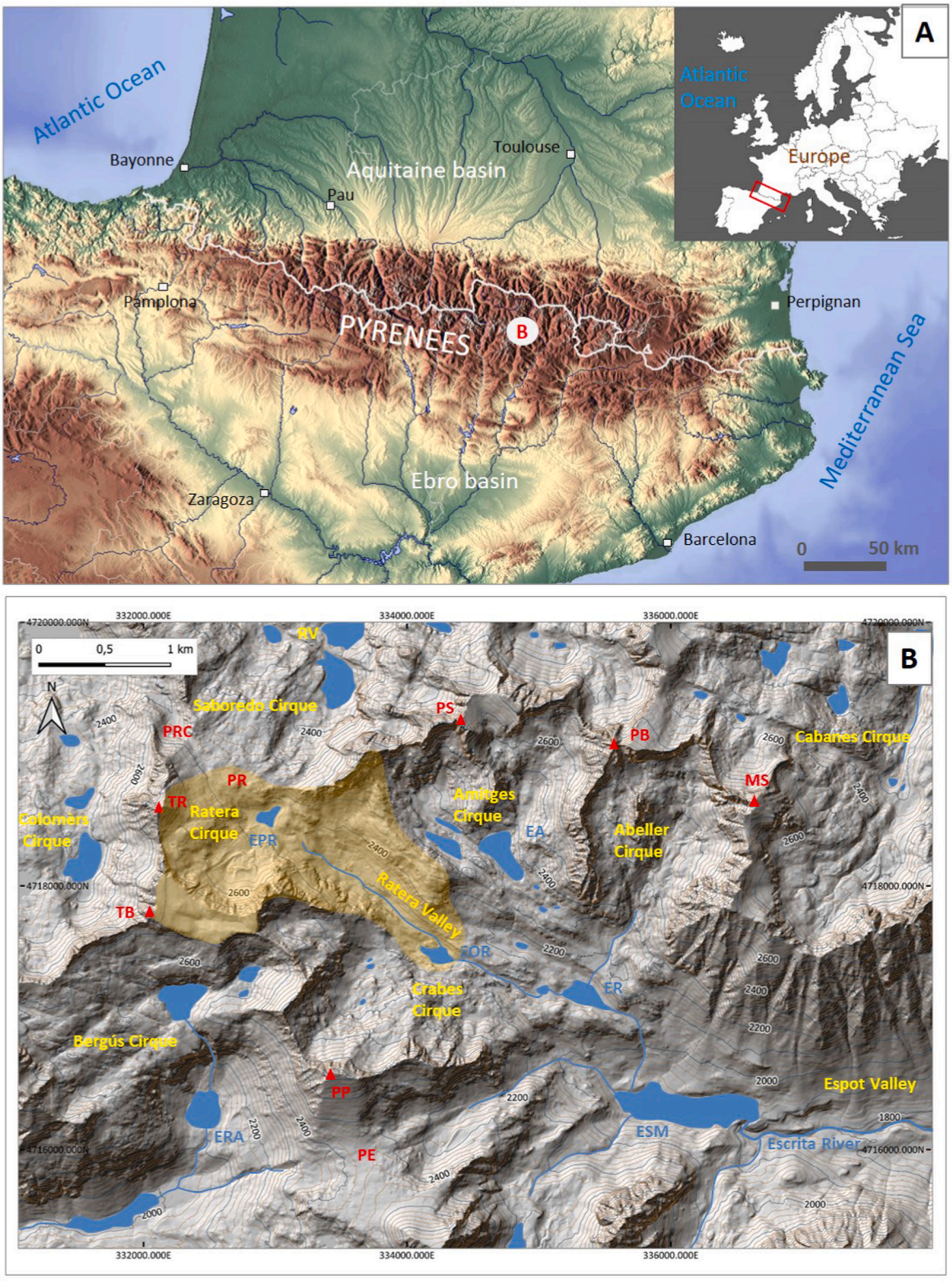

Fig. 1. Map of the study area. (A) Location of Comalesbienes-Colomèrs-Bassiero Massif in the context of the Pyrenees (Spain-France); (B) Topographic map of the surroundings of the Ratera Valley and cirque (eastern sector of the massif). MS= Montsaliente Peak (2890 m); PB = Bassiero Peak (2903 m); TR = Ratera Peak (2861 m); PS = Saboredo Peak (2830 m); TB = Bergús Peak (2843 m); PP = Portarró Peak (2734 m); PR = Ratera Col (2542 m); PE = Portarró d'Espot Col (2427 m); PRC = Ratera de Colomèrs Col (2584 m); RV = Ruda Valley; ESM = Sant Maurici Lake (1915 m); ERA = Redò d'Aigüestortes Lake (2120 m); EPR = Port de Ratera Lake (2470 m); EOR = Obagues de Ratera Lake (2227 m); EA = Amitges Lake (2365 m).
Notes: The area where detailed geomorphological mapping was carried out is delimited in brown (Fig. 2). Contemporary water bodies are shown in blue.

of glacial expansion during the MIS 6, supported by OSL dating of glaciofluvial deposits to 162 ka (Turu et al., 2023), (ii) a local maximum expansion of the LGC that probably occurred during MIS 4 (71-57 ka) based on its own relative chronology correlated with the neighbouring valleys of the Valira and Aran (Ventura and Turu, 2022), (iii) glacial fluctuations during MIS 3 (57-29 ka) and MIS 2 (29-14 ka), based on correlations with glacial landforms formed during T-1 in the adjacent Aran Valley basin (Fernandes et al., 2021, 2023; Oliva et al., 2021), to which the Noguera Pallaresa paleoglacier was connected through two extensive glacial transfluence cols.

3. Methodology

The reconstruction of the deglaciation of the Ratera Cirque and valley was carried out by integrating geomorphological mapping, field observations and the application of geochronological techniques based on ^{10}Be CRE dating on quartz-bearing surface rock samples from different glacial and periglacial landforms.

3.1. Geomorphological mapping

A 1:10,000 scale geomorphological map was produced based on orthophotomaps and digitised after field validation during the summer seasons of 2018 and 2021. A first preliminary map was produced based on the stereoscopic visualisation and interpretation of photograms from different analogue and digital photogrammetric flights carried out by the Institut Cartogràfic i Geològic de Catalunya. This was complemented by other sources, such as Google Earth Pro, digital terrain models with a regular 2 × 2 m grid LIDAR data (MET-2, v.1.0, 2016; https://www.icgc.cat/en/Downloads), to which hillshade was applied, and the high-resolution (25 cm/pixel) RGB and IR digital orthophotos displayed in semi-transparency together with the 1:5000 scale topographic map of Catalonia in the "Vissir3" map viewer (https://srv.icgc.cat/vissir3/). The legend of the geomorphological map was based on the proposal of the Université de Lausanne (Schoeneich, 1993; Lambiel et al., 2013, 2016), which is particularly useful for mountain areas (Pellitero, 2014; Hofmann, 2018). The geomorphological map in Fig. 2 was produced using a DTM-lidar base in hillshade representation, processed in QGIS 3.34.

3.2. Sampling strategy

Based on geomorphological mapping and field evidence, we selected the most suitable landforms to be sampled for CRE dating. Due to the quartz-rich lithology of the area (i.e. granite), the *in-situ* produced cosmogenic nuclide ^{10}Be was selected for CRE dating (Dunai, 2010).

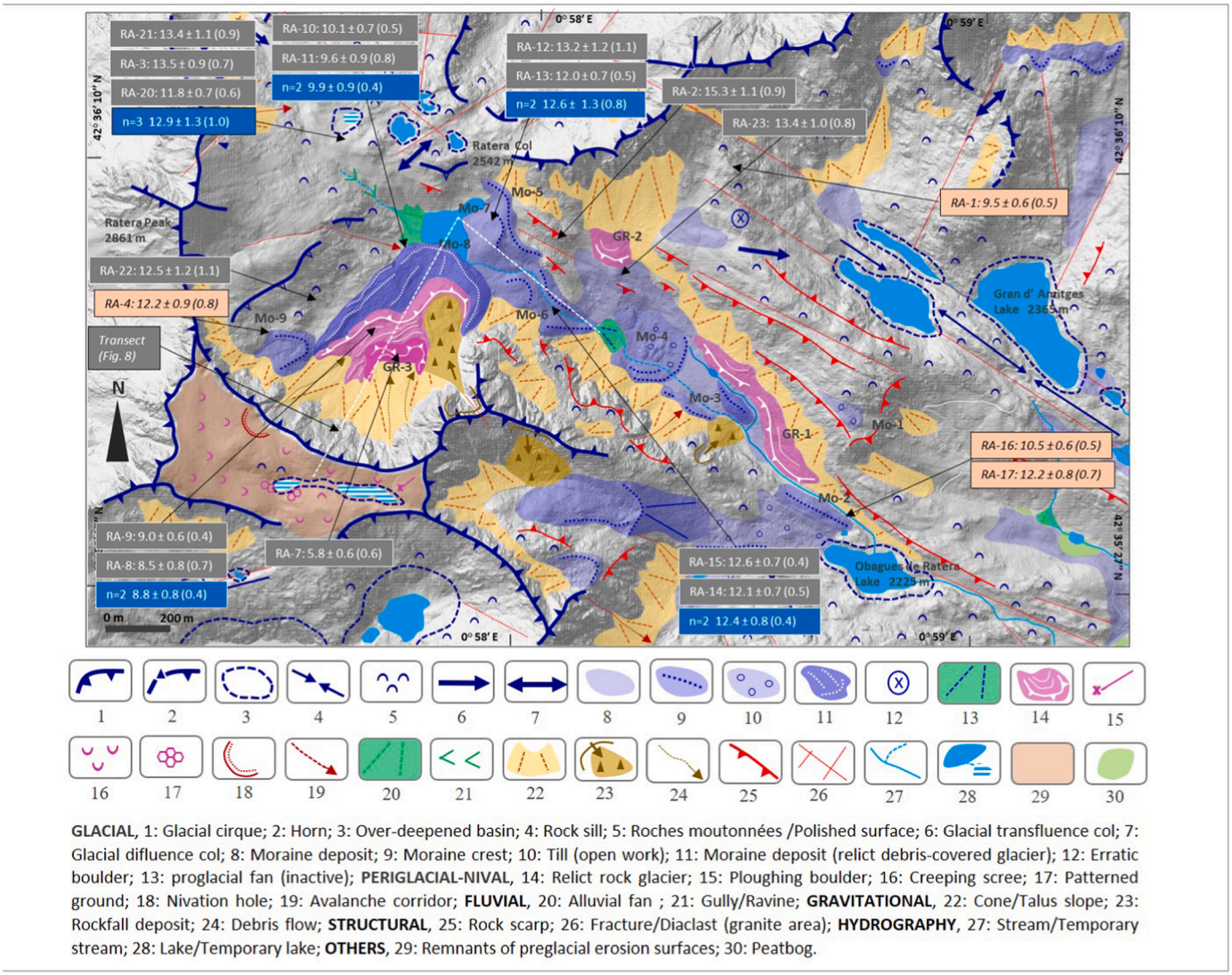

GLACIAL, 1: Glacial cirque; 2: Horn; 3: Over-deepened basin; 4: Rock sill; 5: Roches moutonnées /Polished surface; 6: Glacial transfluence col; 7: Glacial difluence col; 8: Moraine deposit; 9: Moraine crest; 10: Till (open work); 11: Moraine deposit (relict debris-covered glacier); 12: Erratic boulder; 13: proglacial fan (inactive); **PERIGLACIAL-NIVAL**, 14: Relict rock glacier; 15: Ploughing boulder; 16: Creeping scree; 17: Patterned ground; 18: Nivation hole; 19: Avalanche corridor; **FLUVIAL**, 20: Alluvial fan ; 21: Gully/Ravine; **GRAVITATIONAL**, 22: Cone/Talus slope; 23: Rockfall deposit; 24: Debris flow; **STRUCTURAL**, 25: Rock scarp; 26: Fracture/Diaclast (granite area); **HYDROGRAPHY**, 27: Stream/Temporary stream; 28: Lake/Temporary lake; **OTHERS**, 29: Remnants of preglacial erosion surfaces; 30: Peatbog.

Fig. 2. Geomorphological map of the study area including CRE ages (in ka).

In the summer of 2021, 19 samples were collected from moraine boulders (9), rock glacier blocks (3) and glacially-polished bedrock surfaces (7). They were extracted both in the valley and in the cirque, at altitudes between 2273 and 2610 m a.s.l. (Table 1). Using a hammer and chisel, we extracted the uppermost part of the rock (thickness 1.8–5 cm; ~0.7–1 kg) from horizontal or sub-horizontal planes to optimise cosmic ray flux reception (Gosse and Phillips, 2001). The location and size of the sampled features are summarised in Table 1. When sampling bedrock surfaces, we prioritised: (i) exposed outcrops protruding several metres from the surface, and (ii) where possible, with the presence of striations or clear glacial abrasion features. For the moraine boulders, we focused on those at the highest and most stable sectors of the moraine ridges, where the boulders are well anchored and away from the flanks, in order to minimise possible post-glacial denudation processes (burial, overturning, etc.) that could affect the exposure ages obtained. The characteristics of each sampling site (geographical coordinates, substrate type, geomorphological unit, boulder size, sample thickness, strike and dip of the sampled surface …) were noted in the field.

3.3. Laboratory procedures

Physical and chemical treatments of the samples were carried out at the Laboratoire National des Nucléides Cosmogéniques (LN2C) of the Centre Européen de Recherche et d'Enseignement des Geosciences de l'Environnement (CEREGE; Aix-en-Provence, France). Physical processing of samples included: i) crushing and sieving to the 250–500 μm fraction; and ii) the removal of magnetic minerals using the Frantz LB-1 magnetic barrier separator. Later, the chemical processing includes the following steps: i) the removal of the remaining non-quartz minerals (feldspar) by several successive leaches with a concentrated 1:2 mixture of hydrochloric acid (HCl) and hexafluorosilicic acid (H_2SiF_6); ii) the remaining minerals underwent 4–5 partial dissolutions with hydrofluoric acid (HF) to remove atmospheric ^{10}Be and other impurities from quartz; iii) to ensure the purity of the sample, quartz grains were examined using a binocular microscope. As a result, from 18.1 to 25.3 g of pure quartz were extracted per sample; iv) next, 450 μL of ^{9}Be carrier solution (spike, 997 ± 9 μg g^{-1}; obtained from a phenakite crystal) was added to the samples (Merchel et al., 2008), and quartz was finally dissolved in HF; v) Beryllium was separated from other elements in resin exchange columns, first through an anion exchange column (Dowex 1x8) to remove Fe, Mn and Ti, and then through a cation exchange column (Dowex 50Wx8) to discard B and separate Be from other elements (Merchel and Herpers, 1999); vi) the eluted Be was then precipitated to beryllium hydroxide ($Be(OH)_2$), which was oxidised to BeO at 700 °C; and vii) BeO targets were mixed with Nb powder and loaded into copper cathodes, prior to subsequent Accelerator-Mass-Spectrometer (AMS) measurement of ^{10}Be/^{9}Be ratios.

3.4. ^{10}Be age calculations

The measurement of the ^{10}Be/^{9}Be ratio was performed at the 'Accélérateur pour les Sciences de la Terre, Environnement et Risques' (ASTER) of the CEREGE in February 2023. The measurements were calibrated with the internal standard STD- 11, and assigned ^{10}Be/^{9}Be ratio of 1.191 (±0.013) × 10^{-11} (Braucher et al., 2015) and a^{10}Be half-life of 1.387 ± 0.0012 × 10^{6} yr (Chmeleff et al., 2010; Korschinek

Table 1
Geographic location of samples, topographic shielding factor, sample and vertical distance from the summit.

Sample name	Landform		Latitude (DD)	Longitude (DD)	Elevation (m a.s.l.)[a]	Topographic shielding factor	Thickness (cm)
Lowest moraines							
RA-16	Mo-2	Moraine boulder	42.59378	0.97637	2276	0.9757	3.5
RA-17	Mo-2	Moraine boulder	42.59372	0.97665	2273	0.9518	3.5
Polished surfaces (valley)							
RA-1		Polished surface	42.60132	0.97408	2506	0.9905	5.0
Polished surfaces (cirque)							
RA-2		Polished surface	42.60141	0.96663	2495	0.9860	6.0
RA-22		Polished surface	42.59916	0.95908	2565	0.9624	2.8
RA-23		Polished surface	42.59984	0.96981	2386	0.9673	3.0
Polished surfaces (Difluence pass)							
RA-3		Polished surface	42.60419	0.96028	2580	0.9950	5.5
RA-20		Polished surface	42.60368	0.95772	2610	0.9798	1.8
RA-21		Polished surface	42.60439	0.96189	2568	0.9958	2.3
Mouth of the cirque moraines							
RA-12	Mo-7	Moraine boulder	42.60107	0.96545	2486	0.9880	4.5
RA-13	Mo-7	Moraine boulder	42.60067	0.96521	2488	0.9894	4.5
RA-14	Mo-6	Moraine boulder	42.59984	0.96699	2438	0.9816	4.0
RA-15	Mo-6	Moraine boulder	42.59954	0.96707	2433	0.9767	8.0
Moraine (cirque)							
RA-4	Mo-9	Moraine boulder	42.59810	0.95757	2609	0.9671	2.5
Debris-covered glacier (cirque)							
RA-10	Mo-8 (dcg)	Moraine boulder	42.60043	0.96235	2477	0.9776	4.0
RA-11	Mo-8 (dcg)	Moraine boulder	42.60023	0.96214	2479	0.9777	4.0
Rock glacier (cirque)							
RA-7	GR-3 (lower unit)	Rock glacier boulder	42.59761	0.96086	2551	0.9633	4.5
RA-8	GR-3 (upper unit)	Rock glacier boulder	42.59840	0.96062	2539	0.9721	5.0
RA-9	GR-3 (upper unit)	Rock glacier boulder	42.59838	0.96056	2539	0.9720	3.2

[a] Elevations are derived from topographic map 1:5.000 (map viewer Vissir3.35) from Institut Cartogràfic i Geològic de Catalunya (ICGC).

et al., 2010). Results of AMS measurements are presented with their full uncertainties, including the analytical AMS error (in brackets) and that of the production rate (Table 2).

Partial shielding by the surrounding topography was accounted for by implementing the topographic shielding factor; it was calculated for all sampling sites using the ArcGIS toolbox programmed by Li (2018), which implements the routines described in Dunne et al. (1999). It requires a point shapefile of the sampling sites (including strike and dip of the sampling surfaces) and a digital elevation model (DEM). For this study, we used the MDT25 with a 25-m cell size, provided by the Spanish National Centre of Geographic Information (https://centrodedescargas.cnig.es/CentroDescargas/index.jsp) of the Instituto Geográfico Nacional (IGN). Exposure ages were calculated using the CREp (Cosmic Ray Exposure program) online calculator (Martin et al., 2017). To compare the results from our study area with the updated glacial chronology in the Iberian mountains (Oliva et al., 2022), we followed the same criteria: (i) the Lifton-Sato-Dunai (LSD) elevation/latitude scaling scheme (Lifton et al., 2014); (ii) the ERA40 atmospheric model (Uppala et al., 2005); and (iii) the geomagnetic database based on the LSD model (Lifton et al., 2014). We used the production rate at sea level high latitude (SLHL) of 3.98 ± 0.22 atoms per ^{10}Be g^{-1} year^{-1} (Martin et al., 2017). The exposure ages of the samples with their 1σ full and analytical

Table 2
AMS analytical data and exposure ages. 10Be/9Be ratios were inferred from measurements at the ASTER AMS facility. Individual ages are shown with their full uncertainties (including analytical AMS uncertainty and production rate uncertainty) and analytical uncertainty only within brackets. Arithmetic mean ages are given with their full uncertainties and standard deviations within brackets.

Sample name	Landform	Quartz weight (g)	Mass of carrier (^{9}Be mg)	ASTER TEAM cathode number	^{10}Be/^{9}Be (10^{-14})	Blank correction (%)	(^{10}Be) (10^{4} atoms g^{-1})	Age (ka)	Mean age (ka)
Lowest moraines									
RA-16	Mo-2	24.3616	0.465	CLZL	18.687 ± 0.740	3.21	23.08 ± 0.95	10.5 ± 0.6 (0.4)	
RA-17	Mo-2	20.9326	0.465	CLZM	18.168 ± 0.958	3.30	26.07 ± 1.42	12.2 ± 0.8 (0.6)	
Polished surfaces (valley)									
RA-1		23.6623	0.465	CLZJ	19.500 ± 0.849	3.08	24.81 ± 1.12	9.5 ± 0.6 (0.4)	
Polished surfaces (cirque)									
RA-2		25.3830	0.458	IJQU	32.986 ± 2.040	1.62	39.08 ± 2.45	15.3 ± 1.1 (0.9)	
RA-22		22.9637	0.466	CLZQ	25.214 ± 2.138	2.37	33.37 ± 2.90	12.4 ± 1.2 (1.1)	
RA-23		24.8347	0.465	CLZR	26.043 ± 1.491	2.30	31.81 ± 1.86	13.4 ± 0.9 (0.8)	
Polished surfaces (Difluence col)									
RA-3		23.9688	0.457	IJQV	29.614 ± 1.531	1.81	37.07 ± 1.95	13.5 ± 0.9 (0.7)	***1***2.9 ± 1.3 (1.0)
RA-20		24.4338	0.464	CLZN	27.027 ± 1.258	2.22	33.54 ± 1.60	11.8 ± 0.7 (0.6)	
RA-21		23.0547	0.466	CLZO	28.255 ± 1.921	2.12	37.33 ± 2.59	13.4 ± 1.1 (0.9)	
Mouth of the cirque moraines									
RA-12	Mo-7	23.2211	0.465	CLZP	25.896 ± 2.142	2.31	33.85 ± 2.87	13.2 ± 1.2 (1.1)	12.6 ± 1.3 (0.8)
RA-13	Mo-7	22.8992	0.458	IJRD	23.642 ± 0.952	2.26	30.87 ± 1.27	11.9 ± 0.7 (0.5)	
RA-14	Mo-6	21.5995	0.458	IJRE	21.691 ± 0.878	2.47	29.94 ± 1.24	12.1 ± 0.7 (0.5)	12.4 ± 0.8 (0.4)
RA-15	Mo-6	25.1923	0.463	CLZK	24.843 ± 0.741	2.42	29.79 ± 1.08	12.6 ± 0.7 (0.4)	
Moraine (cirque)									
RA-4	Mo-9	24.6688	0.456	IJQW	28.055 ± 1.800	1.92	33.95 ± 2.22	12.2 ± 0.9 (0.8)	
Debris-covered glacier (cirque)									
RA-10	Mo-8 (dcg)	23.6636	0.458	IJRB	20.338 ± 0.911	2.63	25.61 ± 1.18	10.1 ± 0.7 (0.5)	9.9 ± 0.9 (0.4)
RA-11	Mo-8 (dcg)	22.1189	0.458	IJRC	18.238 ± 1.424	2.93	24.50 ± 1.97	9.6 ± 0.9 (0.8)	
Rock glacier (cirque)									
RA-7	GR-3 (lower unit)	21.8748	0.458	IJQY	11.221 ± 1.151	4.78	14.94 ± 1.61	5.8 ± 0.6 (0.6)	
RA-8	GR-3 (upper unit)	23.6784	0.457	IJQZ	18.034 ± 1.398	2.98	22.56 ± 1.80	8.5 ± 0.8 (0.7)	***8.***8 ± 0.8 (0.***4)***
RA-9	GR-3 (upper unit)	18.1069	0.455	IJRA	14.795 ± 0.568	3.65	23.92 ± 0.96	8.9 ± 0.6 (0.4)	

uncertainties are given in Table 2.

In addition, postglacial erosion was corrected with a conservative rate of 1 mm ka^{-1}, representative of the biotite-rich crystalline rock type (André, 2002). The effect of snow cover was also considered (Table 3), with an average snow thickness of ca. 1 m, a snow density of 0.2 g cm^{-3} and a duration of 7 months at 2200–2300 m a.s.l., according to data from the Bonaigua meteorological station (Servei Meteorològic de Catalunya, 1997–2023). Here, we assume the snow cover thickness and duration remained broadly similar to today throughout the last deglaciation. The snow shielding factor was calculated using eq. (3.76) in Gosse and Phillips (2001). The effect of both corrections resulted in ~8.6 % older ages (~1.6 % and ~7.3 % due to erosion correction and snow shielding, respectively; see Table 3). However, to facilitate comparison with published results from other areas, uncorrected ages are presented and discussed in the text.

Finally, the chi-squared test according to Ward and Wilson (1978) was applied to the samples of each geomorphological unit in Fig. 5 to detect potential outliers for exposure age (i.e. 'too old' or 'too young'; Heyman et al., 2011). In our dataset, no outliers were detected using this method (Table 2).

Table 3
Exposure ages acording to erosion and snow cover corrections.

Sample name	Landform	Exposure ages (ka)			
		No correction	Erosion correction	Snow correction	Erosion + snow correction
Lowest moraines					
RA-16	Mo-2	10.5 ± 0.6 (0.5)	10.6 ± 0.6 (0.5)	11.3 ± 0.7 (0.5)	11.4 ± 0.7 (0.5)
RA-17	Mo-2	12.2 ± 0.8 (0.7)	12.3 ± 0.8 (0.7)	13.1 ± 0.9 (0.7)	13.3 ± 0.9 (0.7)
Polished surfaces (valley)					
RA-1		9.5 ± 0.6 (0.5)	9.6 ± 0.6 (0.5)	10.2 ± 0.7 (0.5)	10.3 ± 0.7 (0.5)
Polished surfaces (cirque)					
RA-2		15.3 ± 1.1 (0.9)	15.5 ± 1.1 (0.9)	16.3 ± 1.2 (1.0)	16.6 ± 1.2 (1.0)
RA-22		12.5 ± 1.2 (1.1)	12.6 ± 1.2 (1.1)	13.4 ± 1.3 (1.1)	13.5 ± 1.3 (1.1)
RA-23		13.4 ± 1.0 (0.8)	13.6 ± 1.0 (0.8)	14.4 ± 1.0 (0.8)	14.6 ± 1.0 (0.8)
Polished surfaces (Difluence col)					
RA-3		13.5 ± 0.9 (0.7)	13.7 ± 0.9 (0.7)	14.5 ± 0.9 (0.7)	14.7 ± 0.9 (0.7)
RA-20		11.8 ± 0.7 (0.6)	12.0 ± 0.8 (0.6)	12.7 ± 0.8 (0.6)	12.8 ± 0.8 (0.6)
RA-21		13.4 ± 1.1 (0.9)	13.5 ± 1.1 (0.9)	14.3 ± 1.1 (0.9)	14.5 ± 1.1 (1.0)
Mouth of the cirque moraines					
RA-12	Mo-7	13.2 ± 1.2 (1.1)	13.4 ± 1.2 (1.1)	14.1 ± 1.3 (1.1)	14.3 ± 1.3 (1.2)
RA-13	Mo-7	12.0 ± 0.7 (0.5)	12.1 ± 0.7 (0.5)	12.8 ± 0.7 (0.5)	13.0 ± 0.8 (0.5)
RA-14	Mo-6	12.1 ± 0.7 (0.5)	12.3 ± 0.7 (0.5)	13.0 ± 0.8 (0.5)	13.2 ± 0.8 (0.5)
RA-15	Mo-6	12.6 ± 0.7 (0.4)	12.7 ± 0.7 (0.5)	13.5 ± 0.7 (0.5)	13.6 ± 0.7 (0.5)
Moraine (cirque)					
RA-4	Mo-9	12.2 ± 0.9 (0.8)	13.4 ± 0.9 (0.8)	13.1 ± 1.0 (0.8)	13.30 ± 1 (0.8)
Debris-covered glacier (cirque)					
RA-10	Mo-8 (dcg)	10.1 ± 0.7 (0.5)	10.2 ± 0.7 (0.5)	10.9 ± 0.7 (0.5)	11.0 ± 0.7 (0.5)
RA-11	Mo-8 (dcg)	9.6 ± 0.9 (0.8)	9.7 ± 0.9 (0.8)	10.4 ± 1.0 (0.9)	10.5 ± 1.0 (0.9)
Rock glacier (cirque)					
RA-7	GR-3 (lower unit)	5.8 ± 0.6 (0.6)	5.8 ± 0.6 (0.6)	6.2 ± 0.6 (0.7)	6.2 ± 0.6 (0.6)
RA-8	GR-3 (upper unit)	8.5 ± 0.8 (0.7)	8.6 ± 0.8 (0.7)	9.2 ± 0.9 (0.8)	9.3 ± 0.9 (0.8)
RA-9	GR-3 (upper unit)	9.0 ± 0.6 (0.4)	9.0 ± 0.6 (0.4)	9.7 ± 0.6 (0.4)	9.7 ± 0.6 (0.4)

3.5. Glacier reconstruction and Equilibrium Line Altitude calculation

We used the "PaleoIce" ArcGIS toolbox programmed by Li (2023) to reconstruct the Ratera paleoglacier in 3D for the different glacial phases for which absolute dates are available. This tool requires the glacier flow lines, the approximate geometry of the paleoglacier (derived from frontal and lateral moraines and other mapped geomorphological features) and a DEM. A standard value of 100 kPa for shear stress was applied along the flowline to estimate former ice thickness for each glacial phase, assuming perfect plasticity (Benn and Hulton, 2010). ELAs were calculated from the paleoglacier DEMs using the ELA toolbox included in the PalaeoIce toolbox, taking into account the AABR (Area Altitude Balance Ratio) (BR = 1.75 ± 0.71; Rea, 2009) and AAR (Accumulation Area Ratio) (AAR = 0.6 ± 0.5; Porter, 1975) methods. Note that resulting ELA values can be highly sensitive to the choice of these parameters. The values chosen here were selected to remain consistent, and ease comparison with, previous studies from the region (Fernandes et al., 2021; Oliva et al., 2021).

4. Results

The geomorphological map shows the presence of a wide variety of landforms in the study area, revealing a complex deglaciation sequence during the transition from glacial to periglacial conditions.

4.1. Geomorphological evidence and sampling strategy

The headwaters of the ancient Ratera Glacier comprise two distinct areas: the Ratera Valley and the Ratera Cirque (Figs. 2 and 5). The list of CRE samples collected in each area is given in Table 1.

4.1.1. The Ratera Valley

The Ratera Valley extends for 2.6 km between the edge of the cirque (2455 m a.s.l.) and the Ratera lake (2130 m a.s.l.; Fig. 1B). The lower part of the valley narrows below the Obagues de Ratera lake (2227 m a.s.l.; Fig. 1B), where large longitudinal rock outcrops with traces of glacial abrasion protrude 20–40 m above the valley floor. Its upper part includes debris-covered slopes on the left bank and a flat bottom up to 2300 m a.s.l. The following major glacial and periglacial features are found in this area.

- In the NE boundary of the valley, there are polished bedrock surfaces with remnants of moraine ridges (Mo-1) defined by angular blocks in an openwork structure and large erratic boulders (Ø 4–5 m) on the divide (Figs. 3A and 4C). Sample RA-1 was obtained from the highest part of the exposed outcrop showing glacial striations, at the foot of the ridge of the West Saboredo peak (2762 m a.s.l.).
- At the mouth of the valley, above the Obagues de Ratera lake basin, a 6–12 m high moraine (Mo-2) stretches 270 m between 2283 and 2246 m a.s.l. The alignment of Mo-2 does not clearly indicate whether this deposit was formed by a former glacier descending from the Ratera Valley or from the adjacent Crabes Cirque (Fig. 1B). Two samples were taken from two large, well-anchored boulders of the

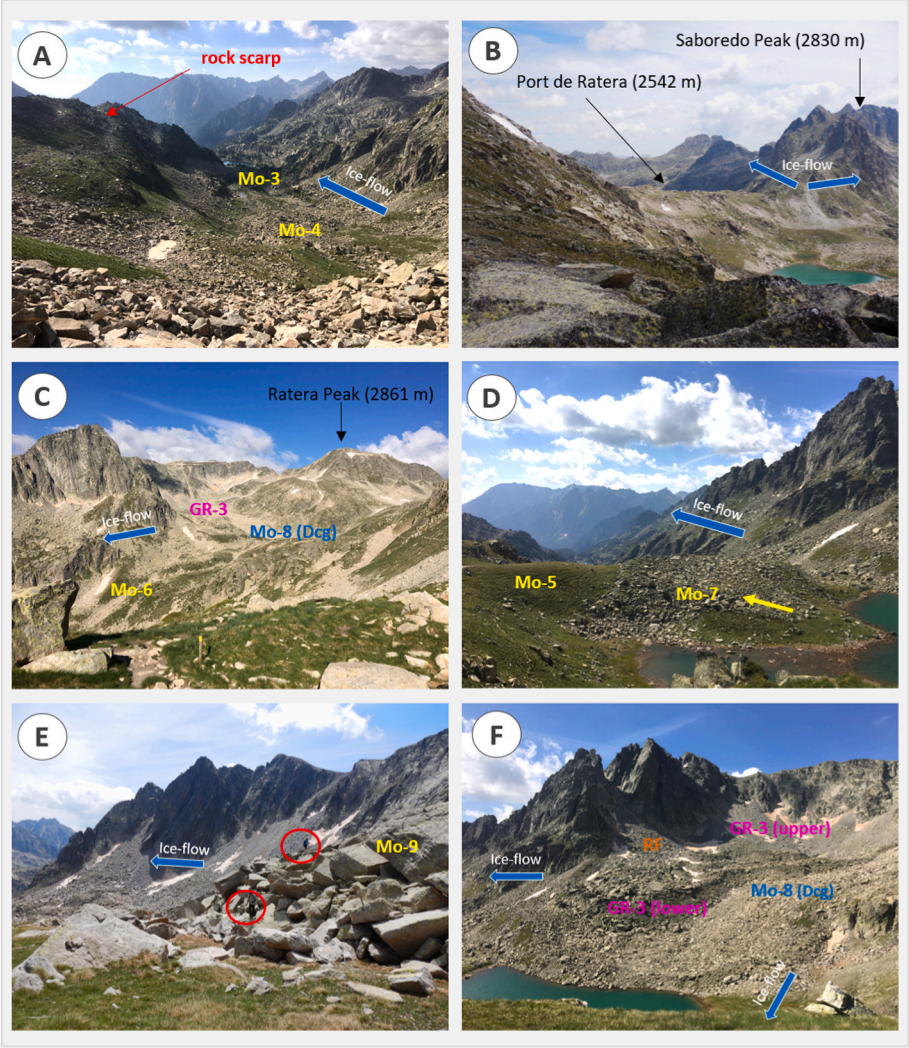

Fig. 3. Examples of the main geomorphological units in the Ratera Cirque-valley: A) view of the Ratera Valley with the moraines (Mo-3 and Mo-4) located at the bottom of the valley; B) glacial difluence col (watershed breach) of Port de Ratera (2542 m); C) general view of the Ratera Cirque; D) detailed view of the push moraine (Mo-7) located above the Mo-5 at the mouth of the Ratera Cirque; E) Left side of moraine Mo-9, the highest in the cirque (2600–2625 m). Two people appear above the reservoir (red circles); and F) Transect inside the Ratera Cirque, Mo-8 (fossil debris-covered glacier) partially covered by a rock glacier with two units (GR-3) and a rockfall above it.

Mo-2 ridge, with no apparent possibility of subsequent translocation (RA-16, RA-17).

- Two lateral moraine remnants are distributed on the right (160 m long and 10 m high) and left (125 m long and 3–5 m high) sides of the flat valley floor with their front at 2300 m a.s.l. (Mo-3) (Fig. 3A).
- A protalus lobe (550 m long and 5–10 m high; GR-1) extends across the left slope of the valley between Mo-3 and Mo-2. This periglacial feature faces SW at an average elevation of 2304 m a.s.l.
- The latero-frontal moraine (Mo-4), located at the bottom of the valley (Fig. 3A), defines a semicircular frontal zone (2310 m a.s.l.), with several small parallel arches (2 m high). While its left ridge extends for ca. 300 m–2375 m a.s.l., the rest of the unit appears largely dismantled with scattered boulders on the surface. Near its summit, a 10 m high front of a south-facing rock glacier (GR-2) lies on a polished bedrock surface at 2390 m a.s.l. Sample RA-23 was collected from a quartz vein located on the same glacially-polished bedrock surface (Fig. 4B).

4.1.2. *The ratera cirque*

This cirque (N-NE exposure) covers an area of 0.9 km^2, with a length of 0.9 km and a maximum width of 1.2 km. The cirque had a double glacial flow: flowing northwards through Port de Ratera (Fig. 1B) towards the Saboredo Cirque (Aran Valley; Fig. 1B) and southwards towards the Ratera Valley (Fig. 3C). The cirque is excavated on the margins of the Bergús erosion paleosurface (2720–2845 m a.s.l.), where the existence of an overdeepened basin and glacially polished bedrock surfaces confirm its glacial occupation during the Quaternary cold periods.

The Port de Ratera (2542 m a.s.l.) defines a 650 m long glacial difluence col that separates the Ratera and Saboredo cirques (Figs. 3B and 4C). Here, the flat surfaces and gentle slopes are dominated by a barren ground, with some abraded outcrops (*roches moutonnées*) and small overdeepened basins defined by the fracture lines. The three samples from Port de Ratera (RA-3, RA-20 and RA-21) were collected from the highest exposed areas of these polished outcrops (Fig. 4C). From 2500 m a.s.l., the slope changes abruptly to the N and descends steeply to the Saboredo Cirque floor. At the NW edge of the col, there is another flat surface (Port de Ratera de Colomèrs, 2584 m), which also favoured the flow of ice from Ratera into the Colomèrs Cirque (Fig. 1B). The glacial and periglacial records identified in the cirque area.

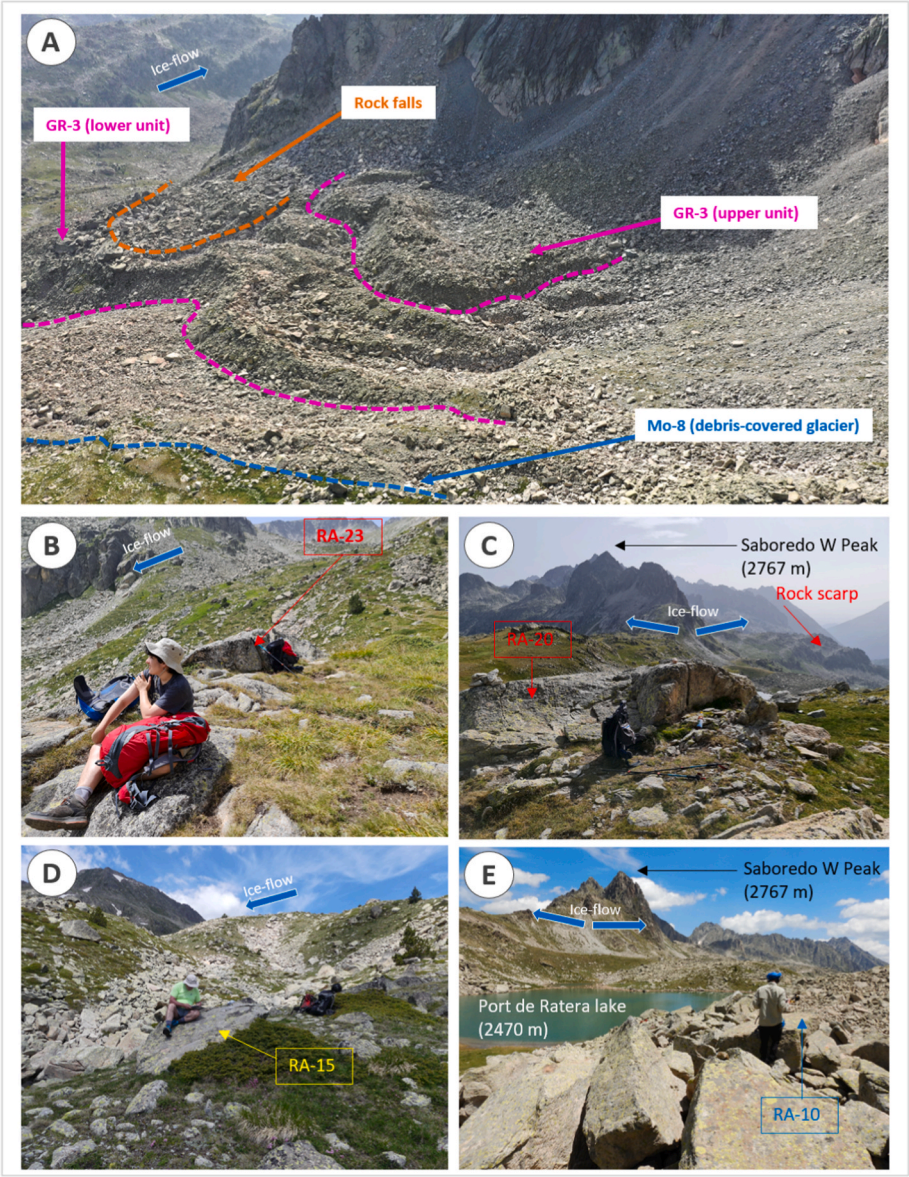

Fig. 4. Examples of the main geomorphological units in the Ratera Cirque-valley: A) Oblique aerial view of the bottom of Ratera Cirque showing the morphology and interrelationship of the fossil debris-covered glacier, rock glacier and rock falls deposits; B) Detail of sample RA-23, located on a polished surface, in the upper area of the Ratera Valley; C) Sample RA-20 (polished surface) located near the Ratera col; D) sample RA-15 (moraine boulder) located on moraine Mo-6; and E) Sample RA-10 (debris-covered glacier boulder) located on the left outer edge of Mo-8.

- Mo-5 is the outermost moraine of this area and occupies the mouth of the Ratera Cirque (Fig. 3D). It corresponds to a (left) lateral moraine starting at 2500 m a.s.l. in a rocky escarpment below the Port de Ratera that descends over 300 m until 2465 m a.s.l. Between Mo-5 and the slopes of the cirque, we found one of the few rocky outcrops in the area with traces of glacial abrasion. Here, we collected sample RA-2, as no suitable boulders were found on the surface of Mo-5.
- At a lower elevation than Mo-5 (2442-2350 a.s.l.), Mo-6 (Fig. 3C) defines a fronto-lateral moraine with two segments, one on each side of the thalweg (235 m long, 8 m high; 190 m long, 15 m high). The Mo-6 samples (RA-14, RA-15) were obtained from large boulders well anchored in the upper part of the moraine ridge (Fig. 4D).
- Closing the Port de Ratera lake (Fig. 1B) to the east, another frontal moraine (Mo-7) extends 200 m between 2488 and 2415 m a.s.l. Around the lake, this moraine expands over the Mo-5 (push moraine) (Fig. 3D). We collected two samples (RA-12 and RA-13) from large stable blocks from the crest of the deposit.
- Another moraine ridge (Mo-8) is located on the southern shore of Port de Ratera Lake at 2475 m a.s.l. (Figs. 3F and 4A). Its steep frontal and lateral slopes (up to 25 m high; 6 m at the lakefront and 2–3 m on the western side) enclose a large deposit of moraine material.
- This deposit consists of clast-supported till with large angular boulders arranged in longitudinal furrows and mounds with block accumulations, and small ridges, features characteristic of the supraglacial mantle of a fossil debris-covered glacier. Large blocks (4–8 m in length) are visible along the ridges, with a central deposit thickness of ~30 m. Similar deposits have been documented elsewhere in the Pyrenees (Andrés et al., 2018; Ventura, 2020; Fernandes et al., 2022) and in other mountain ranges (Zasadni et al., 2020; Balaban et al., 2024), where they are associated with phases of glacier recession.
- At the front of Mo-8, near the lake, two samples were taken from large horizontal boulders (RA-10, RA-11; Fig. 4E). Towards the

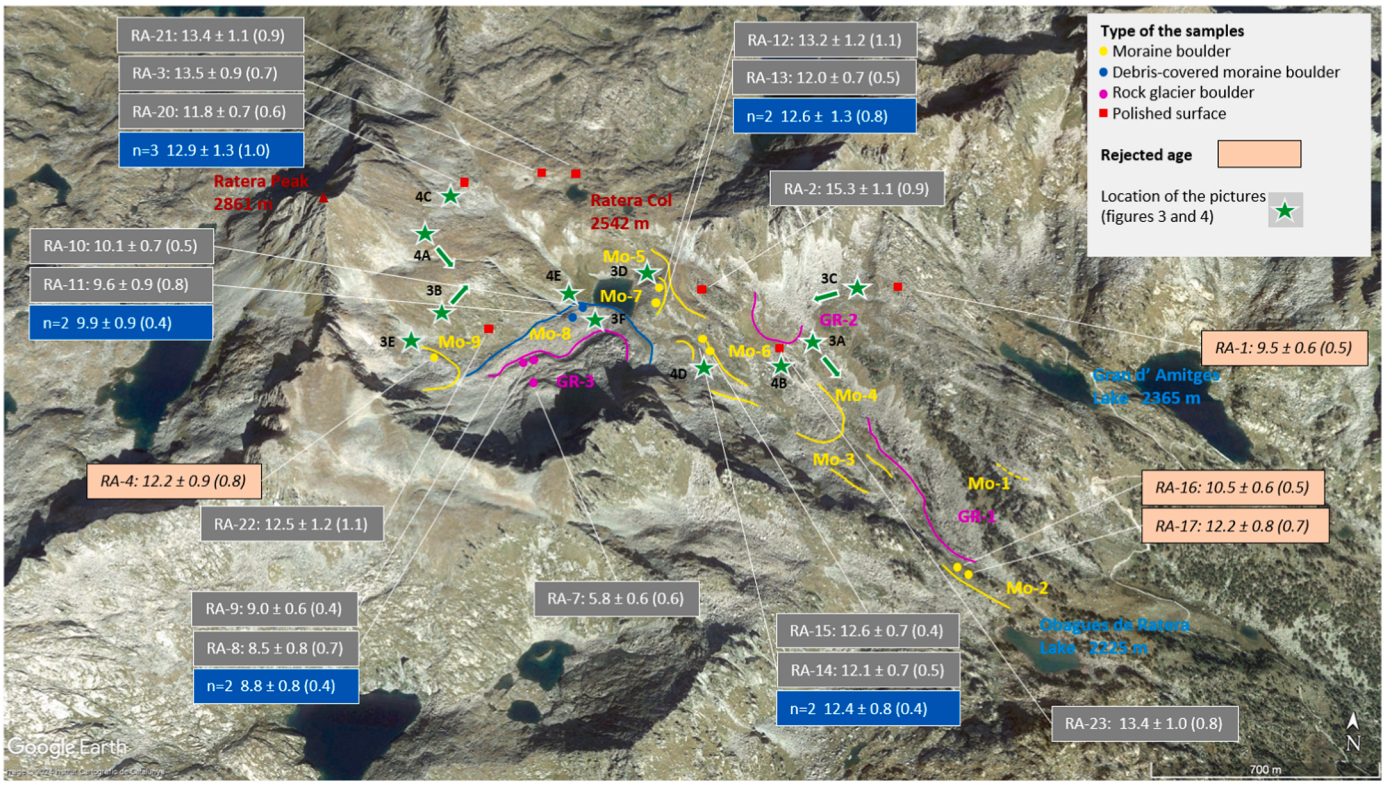

Fig. 5. 3D view (Google Earth) of the study area showing the location of key features and samples. Ages in the image (grey rectangle) reported for the 'no correction' scenario. The mean age of each formation is indicated by a blue rectangle, and with brown rectangle the rejected ages. The location of the pictures in Figs. 3 and 4 are also included.

interior of the cirque and 20 m above its floor, a glacially polished outcrop was sampled (RA-22).

- A rock glacier (GR-3) with a lobate morphology is located below the northern walls of the cirque at 2522 a.s.l. It preserves the characteristic steep front (22 m high), well-contoured sides and the presence of transverse arches and furrows between them (3–8 m high). It is 230 m long and 330 m wide and covers an area of 0.063 km^2 (Figs. 3F and 4A). According to the RGIK (2023) guidelines, it is a multi-unit rock glacier system, with two main units with similar sedimentological characteristics (Fig. 4A): a lower deposit located at 2483–2534 m a.s.l. and an upper one at 2534–2560 m a.s.l. Vegetation is sparse and limited to small patches of *Festuca sp.* on the outer slopes and lichens on the boulders. The outer front of the upper unit is abrupt, unstable and high (12 m), with wet areas of fine-grained sediments on the slopes and a sparse presence of lichens, as well as small seasonal pools within the ridges. GR-3 partially fossilises the deposits corresponding to the abovementioned collapsed debris-covered glacier. Samples from GR-3 were taken from large and stable boulders on the outer ridge of the lower (RA-8, RA-9) and upper (RA-6, RA-7) units.
- The fronto-lateral moraine (Mo-9) at 2600–2625 m a.s.l. defines a 250 m long ridge composed of large angular boulders (Fig. 3E). Two samples for CRE dating were collected from large and well-anchored boulders on the moraine ridge (RA-4, RA-5). Mo-9 partially overlies the collapsed debris-covered glacier deposit. At present, snow patches generally remain in its interior until mid-summer.

4.2. Geochronological data

The 19 samples collected in the Ratera Valley and cirque provide exposure ages spanning a period of 9.5 kyr (between 15.3 ± 1.1 ka and 5.8 ± 0.6 ka), covering the late HS-1 to the Mid-Holocene. In general, the ages show a stratigraphically-coherent sequence, with the oldest being in the areas furthest from the headwaters, as well as in the upper part of the valley near the valley divides (Figs. 5 and 6).

The oldest samples, RA-02 (15.3 ± 1.1 ka) and RA-23 (13.4 ± 1.0 ka), correspond to sectors of glacially abraded bedrock surfaces located in the upper part of the valley and towards the mouth of the cirque. Another group consisting of three samples collected on glacially-polished bedrock surfaces at the Port de Ratera divide provide a new logical geochronological sequence; RA-3 (13.5 ± 0.9 ka), RA-20 (11.8 ± 0.7 ka) and RA-21 (13.4 ± 1.1 ka), with a mean age of 12.9 ± 1.3 ka.

The two sets of samples in the moraines at the mouth of the cirque yielded very close ages, with mean ages of 12.4 ± 0.8 ka for Mo-6 (RA-14: 12.1 ± 0.7 ka; RA-15: 12.6 ± 0.7 ka) and 12.6 ± 1.3 ka for Mo-7 (RA-12: 13.2 ka ±1.2 ka; RA-13: 12.0 ± 0.7 ka). Within the cirque, the moraine associated to the former debris-covered glacier and the two rock-glacier deposits yielded a chronostratigraphically and statistically consistent set of ages. Samples RA-10 (10.1 ± 0.7 ka) and RA-11 (9.6 ± 0.9 ka) in the debris-covered glacier (Mo-8) yielded a mean age of 9.9 ± 0.9 ka. In the lower unit of the rock glacier, two samples (RA-8: 8.5 ± 0.8 ka; RA-9: 9.0 ± 0.6 ka) gave a mean age of 8.8 ± 0.8 ka. Finally, the only available sample from the upper unit of the rock glacier (RA-7) gave an age of 5.8 ± 0.6 ka.

Within the cirque, and above its floor, sample RA-22 at the polished bedrock surface yielded an age of 12.5 ± 1.2 ka, and RA-4 from the small Mo-9 moraine below the cirque walls yielded 12.2 ± 0.9 ka.

4.3. Reconstruction of ELAs

The geomorphological analysis and the CRE results allow us to distinguish three glacial phases in the Ratera area. For each of these phases we have carried out a spatial reconstruction of the paleoglaciers and calculated the corresponding ELAs. There were no major differences between the YD phases, as for both scenarios, our reconstructions produce estimated paleo ELAs of ca. 2589 m a.s.l., with glaciers 1.3 and 1

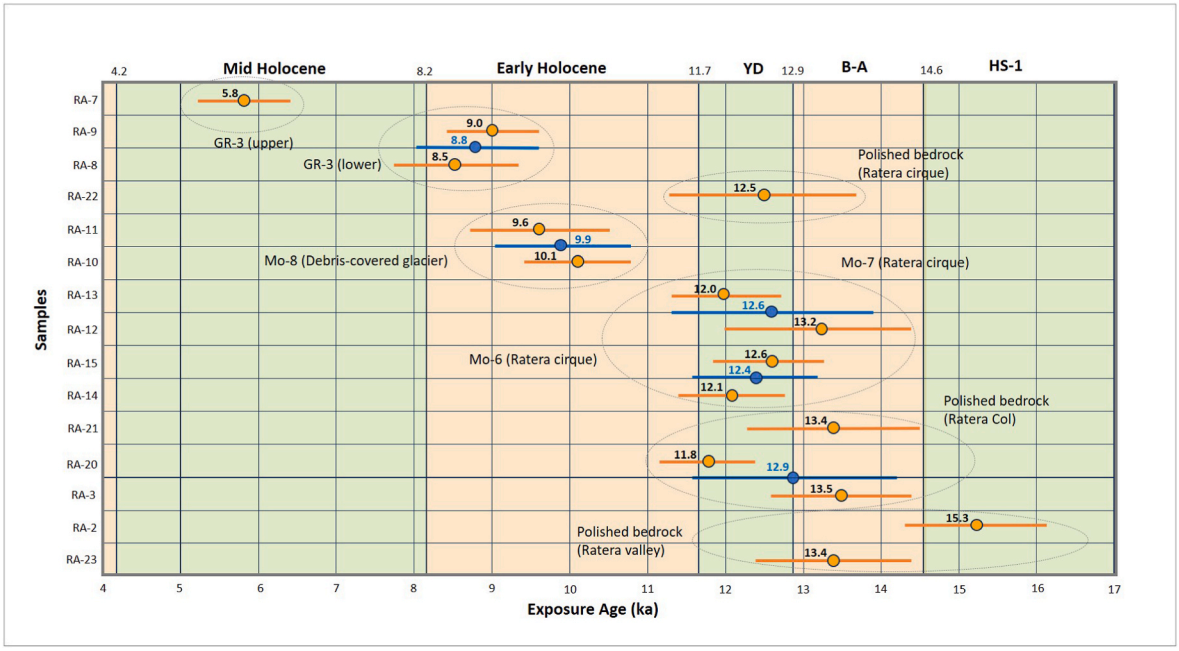

Fig. 6. Clustering of samples by landform and CRE age (in ka), including uncertainties. Mean ages are shown in blue. The orange and green colors help to better visualize the different periods in the figure.

km long, and a maximum thickness of 140 and 90 m, respectively. During the Early Holocene, prior to the glacier becoming debris-covered and while forming the Mo-8 moraine, our reconstruction indicates it was approximately 700 m in length and 80 m thick, with the ELA situated around 2601 m a.s.l. (Fig. 7). However, it is important to emphasize that this ELA estimate is sensitive to the selected SMB profile parameters and basal shear stress values. Fig. 7

5. Discussion

The integration of the ^{10}Be exposure ages with the detailed geomorphological mapping allows us to reconstruct the deglaciation in the Ratera Valley and cirque, including several phases of glacier regrowth/stabilisation and glacier retreat. During this sequence, the glacier evolved from a debris-free glacier to a debris-covered glacier as increasing amounts of debris were incorporated from the cirque walls, both from newly exposed surfaces following glacier thinning and from upper slopes undergoing intensified periglacial activity. This chronology also determines the moments of stabilisation of the two units of rock glacier superimposed on the debris-covered glacier. The period analysed covers the middle and late part of T-1, from the end of HS-1 to the middle of the Holocene.

5.1. Geochronological validity of the results

In the sample dataset we found four samples that are considered

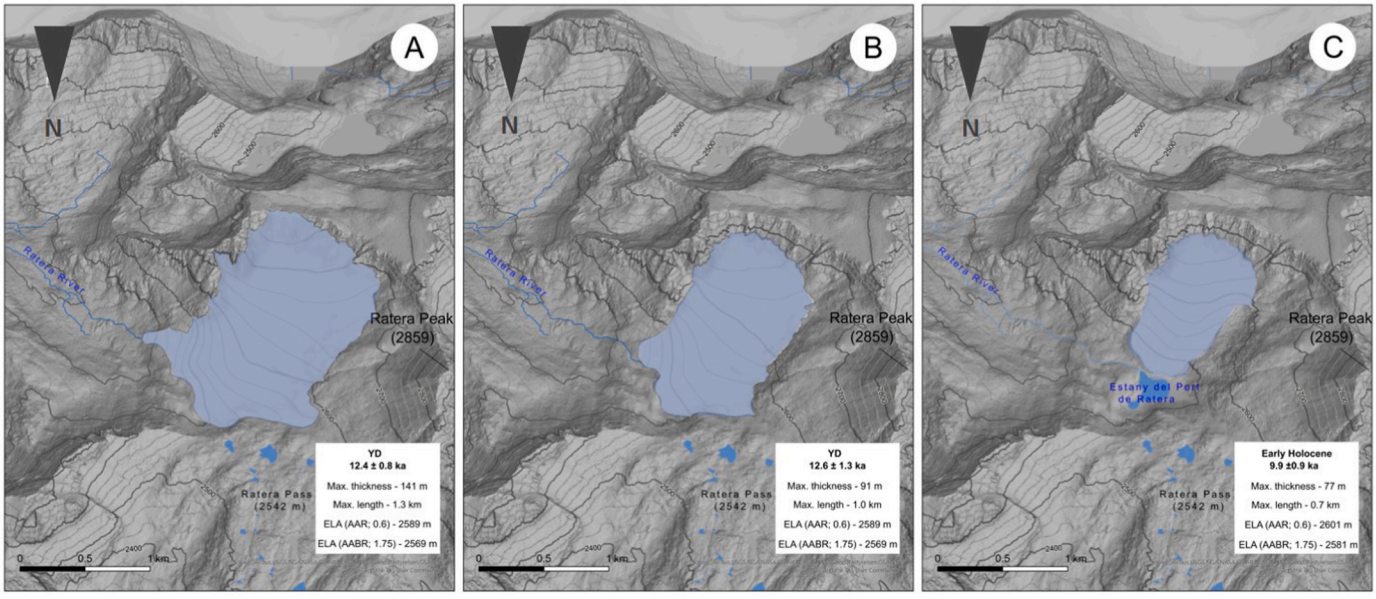

Fig. 7. Paleoglacier reconstruction of the different stages: (A) glacier extent during the YD (12.4 ± 0.8 ka); (B) glacier extent during YD (12.6 ± 1.3 ka); and (C) small glaciers during the Early Holocene (9.9 ± 0.9 ka). The orientation of this figure (to the south) is different from that of the rest of the maps.

geomorphological outliers and for this reason are discarded for the discussion of the results. Samples RA-1 (9.5 ka ±0.6 ka) at the transverse bedrock surface, and RA-16 (10.5 ± 0.6 ka) and RA-17 (12.2 ± 0.8 ka) from the Mo-2 moraine, are not consistent with the logical geochronological sequence of the area as they yielded significantly younger ages. Most likely, these ages may indicate the age of exhumation of the moraine boulders, rather than glacial retreat or deposition. Sample RA-4 from the Mo-9 moraine yielded an age of 12.2 ± 0.9 ka, which is much older than the partially fossilised Mo-8 moraine of the debris-covered glacier (mean age 9.9 ± 0.9 ka). We consider that the age of RA-4 could be influenced by the possible occurrence of nuclide inheritance from previous exposure of the bedrock surface in the cirque wall.

For the rest of the 15 samples, the CRE dates show a consistent geochronological sequence that allows us to infer the spatio-temporal pattern of deglaciation in the Ratera Cirque.

5.2. Chronology of deglaciation in the Ratera cirque and valley

The oldest ages in the Ratera Cirque correspond to the samples RA-2 and RA-23 in the glacially polished surfaces in the upper part of the valley, with exposure ages between 15.3 ± 1.1 ka and 13.4 ± 1.0 ka respectively. These ages indicate a gradual deglaciation of the valley since the end of the HS-1 and during the B-A, in agreement with temperature increases (3–5 °C) detected regionally in Western Europe (Naughton et al., 2023b). This is also consistent with results obtained in other nearby valleys, such as the Ruda and Bacivèr valleys (Fernandes et al., 2021; Oliva et al., 2021), and in other sites in the Pyrenees, where local glaciers experienced substantial deglaciation at the end of the HS-1 and during the B-A, and either disappeared or retreated to the highest parts of the valleys (Delmas et al., 2023b). This pattern has been observed in several other mid-latitude mountains where cirque deglaciation occurred at ca. 14–15 ka (Palacios et al., 2020).

Since then, the prevailing climate conditions favoured periods of minor glacier expansion and stabilisation within the long-term retreat. In the Ratera Valley, this is confirmed by three moraine systems distributed at 2225 and 2380 m a.s.l. (Mo-2, Mo-3 and Mo-4; Figs. 2 and 5), indicating paleoglacier lengths of 2.3, 1.9 and 1.6 km respectively, which represent between 3.6 and 2.5 % of the maximum length extension of 63 km (in the LGC) reached by the Noguera Pallaresa paleoglacier during the MIS 4 (Ventura and Turu, 2022). Considering the sample RA-23, the development of Mo-2, Mo-3 and Mo-4 must have formed earlier than 13.4 ± 0.9 ka, while Mo-5 could have developed after this time. The length of these paleoglaciers was similar to those in the nearby Ruda Valley (3.2–2.6 km) at during the B-A, between 13.5 ± 0.9 and 13.0 ± 0.8 ka (Fernandes et al., 2021). As the glaciers shrank, rock glaciers developed on the valley slopes (GR-1 and GR-2).

The exposure ages of the glacially polished bedrock surfaces of Port de Ratera suggest that the deglaciation of the difluence col occurred at 12.9 ± 1.3 ka, at the transition between the B-A and the beginning of the YD. This age is consistent with the CRE results from moraines Mo-6 (12.4 ± 0.8) and Mo-7 (12.6 ± 1.3 ka), which showed that ice thinning also favoured the deglaciation of the Ratera Cirque margins.

A glacial expansion associated with the 2–4 °C temperature drop that occurred during the YD (Delmas et al., 2023c; Naughton et al., 2023c; Oliva et al., 2023) favoured the development of three moraines at the mouth of the cirque (Figs. 2 and 8). The outermost corresponds to Mo-5, which was formed by a 1.4 km long glacier, and connects to a rocky step below Port de Ratera. The distribution of the moraines between Mo-6 and the rock outcrops in the upper part of the valley suggests that the glaciers did not occupy the col from the end of B-A to the beginning of YD. This pattern is confirmed by the younger samples obtained by Fernandes et al. (2021) immediately to the N, in the Saboredo Cirque, which correspond to two polished rock surfaces located at the bottom of the cirque (at 2360-2316 m a.s.l.). They yielded an average CRE age of 12.7 ± 0.8 ka and were generated by a 1.5 km long glacier that did not cover the sector north of Port de Ratera.

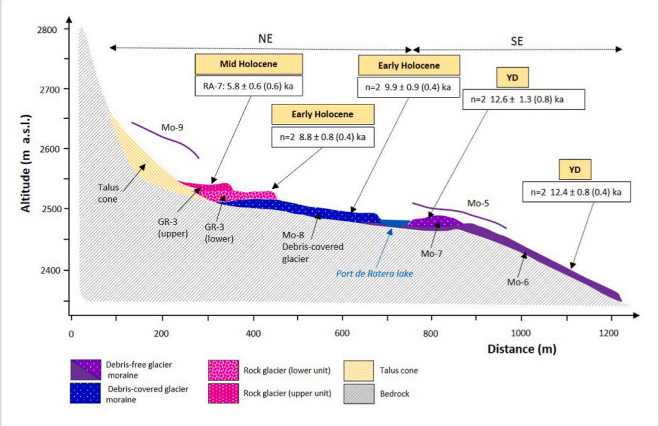

Fig. 8. Geomorphological transect along the Ratera Cirque (towards the NE and E) including the CRE ages (in ka).

Moraines Mo-6 and Mo-7 yielded ages corresponding to the YD (12.4 ± 0.8 ka and 12.6 ± 1.3 ka), with glaciers of 1.3 and 1 km length, respectively, and an ELA of around 2580 m in both cases. The dating of the polished surface within cirque RA-22, with an age of 12.5 ± 1.2 ka, confirms the presence of glaciers in the cirque during the YD. A comparison between the present-day ELA in the Pyrenees, estimated at 3100 m a.s.l. (René, 2011; Jomelli et al., 2020), and the ELA associated with the YD moraines in the Ratera Cirque indicates a decrease of approximately 520 m. This ELA lowering corresponds to an estimated summer temperature decrease of about 3.4 °C, assuming local precipitation remained constant. The extension of the YD glaciers represents only between 2.2 and 1.6 % of the total length of the Noguera Pallaresa paleoglacier during the maximum glacial expansion of the LGC.

Inside the cirque lie the deposits of the collapsed debris-covered glacier (Mo-8; Fig. 8), derived from a 0.7 km-long glacier. The progressive shrinkage of the glacier triggered paraglacial readjustments of the cirque slopes as they became debuttressed and stress was released (Ballantyne, 2002), promoting the transition from a debris-free to a debris-covered glacier. As the ELA rose above the summit line, the upper part of the deposit evolved into a rock glacier. According to Anderson et al. (2018), this transformation results from increasing debris input at the glacier head, its englacial transport, and subsequent emergence at the surface, leading first to debris cover and later to rock-glacier development. Snow from avalanche channels on the cirque walls was incorporated into the ice and mixed with surface debris, further contributing to rock-glacier formation (Anderson et al., 2018). Paraglacial dynamics were particularly intense on the northern walls, where rockfalls and debris flows supplied abundant sediment to the glacier surface. These processes are evidenced by the large blocks on the longitudinal ridges of the debris-covered glacier and on the lower rock glacier. The frontal moraine of the debris-covered Ratera Glacier yielded a mean stabilisation age of 9.9 ± 0.9 ka, indicating that the transition into a debris-covered glacier occurred between the Younger Dryas and the Early Holocene. At that time, the ELA of the Ratera Cirque was ~510 m lower than today, corresponding to a summer temperature decrease of about 3.3 °C, assuming precipitation remained at present levels.

The lower ridge of the rock glacier (GR-3), which partially fossilises Mo-8, reported an average age of stabilisation of 8.8 ± 0.8 ka while the only CRE age from the upper ridge gave an age of 5.8 ± 0.6 ka, suggesting its final stabilisation during the Holocene Thermal Maximum. The eastern sector of GR-3 is largely covered by big boulders, which provides evidence of the intensity of paraglacial dynamics in the cirque.

The sequence of glacial deposits in the Ratera Cirque is completed by Mo-9, the highest moraine (2600 m a.s.l.), built by a small glacier 0.3 km long at the foot of the cirque walls. There is no chronology for this moraine, but it must have formed after the development of the debris-

covered glacier (Mo-8) that partly fossilises. In fact, it could have formed during the Early Holocene, in parallel with the formation of the rock glacier, or it might have developed during the last cold phases of the Late Holocene or Neoglacial (García-Ruiz et al., 2020). In other massifs of the Noguera Pallaresa basin (Bassiero, Certascan, Monteixo-Medacorba), cirque moraines have also been identified at similar altitudes, with fronts at 2550–2650 m a.s.l., in northern aspects at the foot of peaks above 2800 m a.s.l. (Ventura, 2017, 2020).

In reconstructing the deglaciation history of the Ratera Valley and cirque, it is important to acknowledge the uncertainties involved in interpreting the paleoclimatic significance of glacier advances inferred from moraines and their dating—particularly when these relate to debris-laden or debris-covered glaciers (Kirkbride and Winkler, 2012; Anderson et al., 2018). In this context, correlating the Ratera data with CRE ages obtained from nearby areas—especially the neighbouring Saboredo Cirque and Ruda Valley—as well as with results from other studies that applied different methodologies, strengthens the proposed interpretation.

Several other sedimentological, geochemical and palynological studies have been carried out in the same massif, complementing the spatial and temporal evolution of the deglaciation of the Ratera Cirque. Copons and Bordonau (1996) cored the Redó d'Aigüestortes lake (2120 m a.s.l.; Fig. 1B) and radiocarbon dated the base of the lacustrine sediments at 13.4 ka BP (16.0–16.4 cal yr BP). This age must be slightly older than the moraine that dams the lake, which was formed by a 1.7 km long glacier that developed in the Bergús Cirque (Fig. 1B). This age correlates with the Mo-2, Mo-3 and Mo-4 moraines in the Ratera Valley. From the same lake, Copons and Bordonau (1996) dated proglacial sediments at 9.2–8.7 ka BP, suggesting the presence of a glacier during the YD in the upper part of the cirque, as has also been reconstructed for the Ratera Cirque.

Calero et al. (2016) analysed sediments from Sant Maurici Lake (1915 m a.s.l.), located 4 km downstream of the Ratera Cirque. The basal mineral sediments were interpreted as originating from glacier that occupied almost the entire lake basin. The onset of organic deposition, dated at 9.7–9.4 ka, was interpreted as the almost complete retreat of the glaciers into the upper basin, as confirmed by CRE ages from the Ratera Cirque.

The study by Rull et al. (2023) in the Basa Nera lake (located 2 km north of the Colomèrs Cirque, 1890 m a.s.l.; Fig. 1B) provided the first continuous regional pollen record from the Late Glacial to the Holocene, with the following phases: (i) during HS-1, deglaciation of the Basa Nera lake area, in a periglacial environment with permafrost and scarce vegetation cover, with a MAAT 6 °C lower than today; (ii) at the beginning of B-A there was a sharp increase in temperature, favouring the expansion of the tree line, followed by a decrease from 14 ka onwards, with the presence of tundra-like vegetation. This colder phase is related to the 13.5 and 13.0 ka glacial events recorded in the neighbouring Ruda Valley (Fernandes et al., 2021); (iii) during the YD, the lacustrine sedimentary sequence shows an abrupt temperature decrease that was interrupted during the Early Holocene, when a sudden temperature increase led to a rapid forest expansion.

5.3. *The glacial evolution of Ratera Valley in the context of the Pyrenees and other mountains in southern Europe*

Glacial advance during the late B-A and YD has been documented in the Pyrenees (Delmas et al., 2023c), as well as in other mountain ranges of the Iberian Peninsula, the Mediterranean and Europe (Oliva et al., 2023), but the total number of investigated sites remains low. In the lower Pyrenean massifs with the highest peaks of 2600–2800 m a.s.l. also contain evidence of a late B-A and early YD glacial advance, with frontal moraines at the mouth of the cirques formed by small glaciers (0.3–2.0 km long). Debris-covered glacier deposits and rock glaciers have also been associated with the late B-A and YD in these massifs (Oliva et al., 2021). The presence of one or the other landform is determined by topography, summit and cirque floor elevations, aspect, lithology, and the degree of activity on the cirque walls (Palacios et al., 2020).

In the vicinity of the Ratera Cirque, there are three glacial cirques with similar geomorphological settings formed below peaks of 2600–2800 m a.s.l.: the Saboredo, Locampo Bacivèr and Cabanes cirques (Fig. 1B). In the Saboredo Cirque, a glacier (2.5 km long) deposited moraines at 2185 m a.s.l at 13.0 ± 0.8 ka, during the late B-A or early YD (Fernandes et al., 2021). Later, the glaciers retreated to the upper parts of the cirque and deposited moraines at 2470 m at 12.6 ± 1.3 ka, which subsequently developed into rock glaciers (Fernandes et al., 2021). In the Locampo Cirque, the moraine closing the cirque at 2210 m a.s.l. yielded an age of 13.2 ± 1.1 ka, late B-A or early YD. The glacier evolved into a debris-covered glacier and finally into a rock glacier that stabilised at 11.9 ± 0.7 ka (Fernandes et al., 2023). However, as reported in this study, the uncertainty range of CRE dating—particularly during cold/warm phases of T-1—often prevents distinguishing closely spaced glacial phases, even when geomorphological evidence indicates separate ice-margin positions. The pattern is similar in the Bacivèr Cirque, whose lower parts became ice-free at 15-14 ka, but small glaciers 0.3 km long produced moraines at 2370–2470 m a.s.l. dated at 13.3 ± 0.9 and 12.8 ± 0.5 ka, i.e., late B-A and early YD (Oliva et al., 2021). Some glaciers also evolved into debris-covered glaciers, whose final stabilisation occurred during the Early Holocene at 7.2 ± 0.5 ka (Oliva et al., 2021). The Cabanes Cirque, located NE of the Ratera Cirque, contains a well-preserved and continuous 2 km glacial transect (Ventura, 2020). This sequence begins with a lateral moraine at 2260 m a.s.l., which is in contact with an extensive area of clast-supported till containing large angular boulders between 2280 and 2345 m a.s.l. Overlying this till is a rock glacier approximately 850 m in length, comprising five distinct units with frontal positions ranging from 2345 to 2505 m a.s.l. At the upper end of the cirque, a boulder-rich moraine closes the basin at 2560 m a.s.l. Although no numerical dating is currently available, relative chronological evidence suggests that the entire transect was formed between the late B-A and the Holocene (Ventura, 2020).

Ca. 40 km to the E of the Ratera Cirque, in the Medacorba Massif, a 1.6 km long glacier created a moraine complex at 2220 m a.s.l. with three moraines that yielded CRE ages of 13.2 ± 0.7 ka (late B-A), 12.4 ka ±0.8 (YD) and 11.3 ± 0.6 ka (Early Holocene). Towards the interior of the cirque, one of the moraine ridges at 2265 m a.s.l. yielded an age of 9.9 ± 0.7 ka, earlier than the formation of the overlying rock glacier (Jomelli et al., 2020). Further E, in the Eastern Pyrenees, at the foot of the N walls of the Sierra del Cadi, two groups of moraines (2.5 and 1.7 km glaciers) have been identified at relatively low altitudes (between 1600 and 2100 m a.s.l.) that have provided CRE ages within the YD; 12.9 ± 1.0 and 12.1 ± 1.1 ka, respectively (Çiner et al., 2024).

On the western fringe of the Central Pyrenees, 95 km W of the Ratera Cirque, is the Brazato Cirque. It presents a sequence of polished surfaces at 2335 m a.s.l. dated at 13.4 ± 0.8 ka (B-A - YD transition; 0.8 km glacier), at 2365 m a.s.l. dated at 10.4 ± 0.6 ka (Early Holocene; 0.6 km glacier), followed by a rock glacier with its front at 2370 m a.s.l. that stabilised at 6.1 ± 0.3 ka in the Middle Holocene (Palacios et al., 2017).

In other cirques of lower altitude and southern orientation, the last deglaciation occurred during the B-A period, when rock glaciers replaced the former glaciers. This is the case of the Puigpedrós Massif, Eastern Pyrenees, where one of the S-facing cirques (2673 m a.s.l.) contains moraines at 2305 m a.s.l. of a 1 km long glacier dated at 14.8 ± 1.6 ka. Deglaciation produced a rock glacier with its front at 2385 m a.s.l., which stabilised in its frontal zone at 14.7 ± 2.0 ka, but its upper ridges were active along the B-A, YD, until the Early Holocene (Andrés et al., 2018).

Most CRE ages from glacial deposits in the highest cirques of the Pyrenees are from the YD and Early Holocene (García-Ruiz et al., 2016; Oliva et al., 2019; Delmas et al., 2023 ab). In the Central Pyrenees, only massifs with peaks >3000 m a.s.l. hosted alpine glaciers with maximum lengths of 3–6 km during the YD. In the Balaitús and Picos del Inferno

massifs, YD glaciers (2.4–6 km long) deposited moraines at 1650–2200 m a.s.l. with CRE ages between 12 and 11 ka (Palacios et al., 2015, 2017). In the Maladeta Massif, the Mulleres Glacier reached a length of 3.8 km with its frontal moraine at 1720 m a.s.l. dated at 13.1 ± 0.9 ka (Pallàs et al., 2006; Delmas et al., 2023), and the Aneto Glacier reaching 2 km in length during the Early Holocene at ca. 10.5 ka (Vidaller, 2025). In the Eastern Pyrenees, the paleoglacier of the Cometa d'Espagne, the Carlit Massif, flowed for 1.1 km and its moraines at 2186 m a.s.l. were dated at 11.5 ± 2.0 ka (Crest et al., 2017; Tomkins et al., 2018).

In other Iberian mountains, there is also geochronological evidence for the expansion of small ice masses during the YD. This is the case of the Cantabrian Range, in the Monasterio Valley, where the highest moraines (1540 m a.s.l.), built by a 1 km long glacier were dated to 14.8 ± 0.5 ka and the overlying rock glacier front to 13.7 ± 0.5 ka (Rodríguez-Rodríguez et al., 2017). In the Sierra de la Demanda (Iberian Range), the stabilisation of two debris-covered glaciers in the cirques of San Lorenzo and Mencilla has been dated by CRE. Their formation occurred during the glacial retreat between LGM and HS-1, but their activity was maintained along the B-A and YD, stabilising in the Holocene at 9.0 ± 0.4 and 6.5 ± 0.3 ka, respectively (Fernández-Fernández et al., 2017), with the stabilisation age controlled by the prevailing glacier aspect, SE and NNE, respectively. In the Iberian Central System, glacially polished surfaces revealed by a small retreating glacier in the Pinar Valley, Gredos Massif, were dated to 10.3 ± 1.3 ka (Palacios et al., 2012a). In the Cuerpo de Hombre Valley (Sierra de Béjar Massif), Carrillo and Ninot (1998) CRE dated a 0.6 km long glacial moraine to 12.1 ± 1.2 ka, and in the Peñalara Cirque (Sierra de Guadarrama), a polished outcrop provided an age of 11.7 ± 0.4 ka, indicating the presence of a small glacier below the ridge during the YD (Palacios et al., 2012b). In the Sierra Nevada, in the south of the Iberian Peninsula, YD and Early Holocene glacial records are widespread in the highest northern cirques below peaks of 2800–3200 m a.s.l. Here, glacially polished surfaces and moraines generated by 0.4–1.2 km long glaciers have been dated to between 12.0 ± 1.1 and 11.1 ± 0.9 ka (Palacios et al., 2016). Many of the inactive rock glaciers distributed in cirque slopes between 2585 and 3025 m a.s.l. formed during the HS-1, and their fronts stabilised between 13.1 ± 1.2 and 9.0 ± 0.8 ka, while their roots remained active until 6.4 ± 0.6 ka, such as in the Dílar Cirque (Palacios et al., 2016).

Along the European continent, glacial expansion during the late B-A and YD has been documented in Fennoscandinavia (Lasberg and Kalm, 2013), the Great Britain and Ireland (Ballantyne, 2010) as well as in many mountain ranges, such as the Alps (Steinemann et al., 2020; Lehmann et al., 2022; Ivy-Ochs et al., 2023), the Carpathians (Zasadni et al., 2020; Urdea et al., 2023; Zasadni et al., 2023a) and also in the Mediterranean alpine ranges: Apennines (Dramis and Kotarba, 1994; Giraudi, 2015; Ribolini et al., 2023), Balkan Mountains (Allard et al., 2020; Hughes et al., 2023), Taurus Mountains and Eastern Black Sea Mountains in Anatolia (Akçar, 2023).

The glacial-periglacial evolution between the Lateglacial and the Holocene shows different sequences across European mountains. In the Carpathian Mountains, there are examples of a transition from glaciers to debris-covered glaciers and rock glaciers, as reported in the Piec Stawów Polskich Cirque (High Tatra Mountains) where a debris-covered glacier (at 1840 m a.s.l.) and four later rock glaciers (at 1890 m a.s.l.) were dated at YD (Zasadni and Kłapyta, 2016). Similarly, in the Retezat Mountains (Southern Carpathians), Ruszkiczay-Rüdiger et al. (2016) reported on the formations located inside the cirques (Pietrele, Galesu and Valea Rea cirques); "moraines with large blocs in open structure" (at 1800–1900 m a.s.l.) dated between 15.0 and 13.5 ka (B-A), glacier-derived rock glaciers (at 1900–2000 m a.s.l.) of YD age and small talus-rock glaciers (at 2100–2150 m a.s.l.) of Early Holocene age. Nearby, in the Godeanu Mountains, Balaban et al. (2024) documented debris-charged cirques associated with a final phase of deglaciation (proposed B-A age), where distinct landforms coexist, including debris-covered glaciers evolving into rock glaciers, talus-derived rock glaciers, and even rock-glacierised lateral moraines.

In other regions, debris-free glaciers evolved directly into rock glaciers as ice masses shrank. This is the case in the Schwarzkar Cirque (Northern Calcareous Alps), where a sequence includes a group of moraines (at 1650 m a.s.l.) of YD age, a fronto-lateral moraine (at 1940 m a.s.l.) with ages 11.0 and 9.9 ka and a rock glacier (at 1975 m a.s.l.) dated at 9.1 ka (Moran et al., 2016b). Similarly, in the Kavron Valley (Eastern Black Sea Mountains), a frontal moraine (at 2890 m a.s.l.) dated to 12.8 ka, is followed by an extensive rock glacier whose lower units in contact with the moraine are considered to be of YD age (Akçar et al., 2007). Table 4 includes a selection of ten localities in the European Mountains that include sequences of deposits in glacial-periglacial transition.

With the exception of the Central Alps, where the YD produced important valley glaciers, the cold conditions that prevailed during the YD did not result in substantial glacier expansion in the rest of the central and southern European mountain ranges, and the typology of glacial deposits is very similar to that described in the cirques of the Pyrenees and the others of the European mountains (Palacios et al., 2020), where the "rock glacier-glacier landscape continuum" sequences (Giardino and Vitek, 1988) abound, evidencing the glacial-periglacial transition that occurred in the European high mountains. Overall, reconstructions from the Pyrenees corroborate work in other regions of Europe, suggesting that YD advances were relatively restricted compared with the magnitude of cooling experienced during that time, as indicate by numerous paleoclimate proxy records. This paradox might indicative different climate regime and perhaps dryer conditions than today in western Europe during the YD and the beginning of the Holocene.

6. Conclusions

This paper focuses on the last deglaciation, during the T-1 and the Pleistocene-Holocene transition in the Ratera Valley (Noguera Pallaresa basin, southern central Pyrenees), combining field observations, geomorphological mapping and 15 CRE ages of the main glacial and periglacial landforms present in the cirque. The chronological sequence offers a rare, detailed record of the final stages of deglaciation in the mountains of southern Europe.

- The deglaciation of the Ratera Valley occurred between 15.3 and 13.4 ka (late HS-1 and B-A). Several moraines formed during the warm B-A period, suggesting periods of glacier stabilisation and small advances within the general retreat pattern. Shrinking of the ice masses favoured the development of rock glaciers.
- The deglaciation of Port de Ratera occurred in the middle of the B-A and the beginning of the YD. During this phase, the colder climatic conditions favoured the development of a glacier inside the cirque, which formed three moraine ridges at ca. 12.6–12.4 ka.
- The Early Holocene warming inferred from the landforms inside the Ratera Cirque favoured glacier shrinkage and enhanced paraglacial activity, with increased slope failure and periglacial dynamics. This promoted firstly the transformation of a debris-free glacier into a debris-covered glacier, which stabilised at 9.9 ka, and then the development of a rock glacier, whose lower ridge stabilised at 8.8 ka and its upper sector at 5.8 ka during the Holocene Thermal Maximum. No chronology is available for the highest cirque moraines, which likely formed during the Mid to Late Holocene.

CRediT authorship contribution statement

Josep Ventura: Writing – review & editing, Writing – original draft, Visualization, Investigation, Formal analysis, Conceptualization. **Marc Oliva:** Writing – review & editing, Writing – original draft, Methodology, Investigation, Funding acquisition, Conceptualization. **José M. Fernández-Fernández:** Writing – review & editing, Writing – original draft, Investigation, Formal analysis. **Marcelo Fernandes:** Writing – review & editing, Writing – original draft, Methodology, Investigation.

Table 4
Location and main characteristics of a selection of cirque/valley areas (in European mountains) with sequences of deposits in glacial-periglacial transition.

Cirque/Valley (Massif)	Elevation (m a.s.l.) and coordinates	Aspect	Distance from headwall to the oldest deposits (m)	Sequence of landforms	Age	References
Mandlkar Cirque	2366	NW	2600	Lateral moraine	Late Glacial	Moran et al. (2016a)
Karwendal Mts.	47°19′19″ N			Moraine (with a rock glacier in the frontal area)		
Northern Calcareous Alps	11°23′54″ E			9 talus rock glaciers	12.2–10.1 ka	
Schwarzkar Cirque	2661	NE	2700	Group of moraines	YD	Moran et al. (2016b)
Mieminger Range	47°21′24″ N			Moraine (fronto-lateral)	11.0–9.9 ka	
Northern Calcareous Alps	10°55′18″ E			Rock glacier	9.1 ka	
Piz Valley	2996	NE	1100	Moraine	2.27–2.48 ^{14}C yr BP	Ribolini et al. (2007)
Argentera Massif	44°17′06″ N			Active rock glacier		
Maritime Alps	06°59′52″ E			LIA moraine, leading to debris-covered glacier		
Kavron Valley	3932	N	2600	Moraine		
Mt. Kaçkar	40°50′01″ N			Moraine (inner frontal)	12.8 ka	Akçar et al. (2007)
Eastern Black Sea Mts.	41°07′46″ E			Rock glacier (with inactive and active units)	Inactive RG: post YD	Akçar (2023)
				Frontal moraine	LIA	Yeşilyurt (2025)
				Rock glacier (in the upper zone)	post-LIA	
Üçker Cirque	3917	E	6800	Till deposits	20.4 ka	
Mt. Erciyes	38°31′45″ N			Till (hummocky morphology)	15.2 ka	Sarikayaet al. (2009)
Anatolia	35°28′05″ E			Rock glacier (fossil)	9.2 ka	
				Moraine	Late Holocene	Akçar (2024)
				Debris-rock glacier (active)		
Piec Stawów	2301	SE	2400	Till (with avalanche rocks on top)	HS1	
Polskich Cirque	49°12′31″ N			Till (boulder-rich ablation moraine)	HS1	Zasadni and Klapyta (2016)
Roztoka Valley	20°01′24″ E			Debris-covered glacier moraine	YD	
High Tatra Mt.				4 rock glaciers	YD	
Vazecka Valley	2494	S	2800	Moraine (with abundant boulder cover)	HS1	Zasadni et al. (2020)
Mt. Krivan	49°09′07″ N			Moraine and till (with large boulders)	14.9 ka	Zasadni et al. (2023b)
High Tatra Mt.	20°00′32″ E			Debris-rock glacier	11.1 ka	
Pietrele, Galesu and	2509	N-NW	1600–1900	Moraine (with large blocs)	15.0–13.5 ka	Ruszkiczay-Rüdigeret al. (2016)
Valea Rea cirques	45°22′50″ N			Glacier-derived rock glacier	YD	
Retezat Massif	22°53′39″ E			Talus-rock glaciers	Early Holocene	Urdea et al. (2023)
Southern Carpatians						Urdea et al. (2024)
Zadna Voda Valley	2024	N	4300	Moraine	LGM	
Demänovska Valley	48°57′20″ N			Debris-covered glacier moraine	HS1	Pyrda (2023)
Low Tatra Mt.	19°34′21″ E			Debris and talus-rock glaciers	Late Glacial	
Scindarella Cirque	2233	N	1100	Moraine	HS1	Giraudi andFrezotti (1997)
Gran Sasso Massif	42°26′07″ N			Rock glacier	YD	
Central Apennines	13°34′52″ E					Ribolini et al. (2023)

David Palacios: Writing – review & editing, Writing – original draft, Investigation, Formal analysis. **Tancrède Leger:** Writing – review & editing, Validation, Methodology, Data curation. **Vincent Jomelli:** Writing – review & editing, Supervision, Methodology, Data curation.

Declaration of competing interest

The authors declare that they have no known competing financial interests or personal relationships that could have appeared to influence the work reported in this paper.

Acknowledgements

This research article has been supported by the CRIOPIRINEUS project (Natural Park of Alt Pirineu - Government of Catalonia) and by the ANTALP research group (Antarctic, Artic, Alpine Environments; 2021-SGR-00269) funded by the Government of Catalonia. The ^{10}Be measurements were carried out at the ASTER AMS National Facility (CEREGE, Aix-en-Provence), supported by the INSU/CNRS and the ANR through the "Projets thématiques d'excellence" programme for the "Équipements d'excellence" ASTER-CEREGE action and the IRD. We would also like to thank Jordi Nofre and Jordi Martín for their assistance in the field. Marc Oliva acknowledges the support received from ICREA Academia (AGAUR-Generalitat de Catalunya).

Data availability

Data will be made available on request.

References

Akçar, N., Yavuz, V., Ivy-Ochs, S., Kubik, P.W., Vardar, M., Schlüchter, C., 2007. Paleoglacial records from Kavron Valley, NE Turkey: field and cosmogenic exposure dating evidence. Quat. Int. 164–165, 170–183.

Akçar, N., 2023. The anatolian Mountains: glacial landforms from the Younger Dryas stadial (chapter 60). In: Palacios, D., Hughes, P., García-Ruiz, J.M., Andre's, A. (Eds.), European Glacial Landscapes: the Last Deglaciation. Elsevier, pp. 581–586.

Akçar, N., 2024. Holocene glacial landscapes of the Anatolian Peninsula. In: Palacios, D., Hughes, P., Jomelli, V., Tanarro, L.M. (Eds.), European Glacial Landscapes: the Holocene. Elsevier, pp. 513–530.

Allard, J.L., Hughes, P.D., Woodward, J.C., Fink, D., Simon, K., Wilcken, K.M., 2020. Late Pleistocene glaciers in Greece: a new 36Cl chronology. Quat. Sci. Rev. 245, 106528.

Anderson, R.S., Anderson, L.S., Armstrong, W.H., Rossi, M.W., Crump, S.E., 2018. Glaciation of alpine valleys: the glacier-debris-covered glacier-rock glacier continuum. Geomorphology 311, 127–142.

André, M.F., 2002. Rates of postglacial rock weathering on glacially scoured outcrops (Abisko-Riksgr€ansen area, 68°N). Geogrr. Ann. Phys. Geogr. 84, 139–150.

Andrés, N., Gómez-Ortiz, A., Fernández-Fernández, J.M., Tanarro, L.M., Salvador-Franch, F., Oliva, M., Palacios, D., 2018. Timing of deglaciation and rock glacier origin in the southeastern Pyrenees: a review and new data. Boreas 47, 1050–1071. https://doi.org/10.1111/bor.12324.

Balaban, C.I., Roberts, D.H., Evans, D.J.A., Jamieson, S.S.R., 2024. Past glaciation of temperate-continental mountains: a model for a debris-charged plateau icefield/cirque glacier landsystem in the Southern Carpathians, Romania. Earth Surf. Process. Landf. 2024, 601–621.

Ballantyne, C.K., 2002. Paraglacial geomorphology. Quat. Sci. Rev. 21 (18–19), 1935–2017. Oct 1. https://www.sciencedirect.com/science/article/abs/pii/S0277379102000057.

Ballantyne, C.K., 2010. Extent and deglacial chronology of the last British-Irish Ice Sheet: implications for exposure dating using cosmogenic isotopes. J. Quat. Sci. 25, 515–534.

Benn, D.I., Hulton, N.R.J., 2010. An Excel TM spreadsheet program for reconstructing the surface profile of former mountain glaciers and ice caps. Comput. Geosci. 36 (5), 605–610. https://doi.org/10.1016/j.cageo.2009.09.016.

Bordonau, J., Serrat, D. y, Vilaplana, J.M., 1992. Las fases glaciares cuaternarias en los Pirineos. En. In: Cearreta, A., y Ugarte, F.M. (Eds.), The Late Quaternary in the Western Pyrenaen Region. Serv. Univ. País Vasco, Bilbao, pp. 303–312.

Braucher, R., Guillou, V., Bourlès, D.L., Arnold, M., Aumaître, G., Keddadouche, K., Nottoli, E., 2015. Preparation of ASTER in- house 10Be/9Be standard solutions. Nucl. Instrum. Methods Phys. Res. Sect. B Beam Interact. Mater. Atoms 361, 335–340.

Bru, J., Gomez Ortiz, A., Serrat, D., Ventura, J., Vilaplana, J.M., 1985. Sintesis de la dinamica glacial cuaternaria en la vertiente meridional del Pirineo Catalan. In: I Reunión Del Cuaternario Ibérico. Lisboa, pp. 165–183.

Buizert, C., Keisling, B.A., Box, J.E., He, F., Carlson, A.E., Sinclair, G., DeConto, R.M., 2018. Greenland-wide seasonal temperatures during the last deglaciation. Geophys. Res. Lett. 45, 1905–1914. https://doi.org/10.1002/2017GL075601.

Calero, M.A., Valero-Garcés, B.L., Rull, V., Vegas-Vilarrúbia, T., Garcés-Pastor, S., López-Vila, J., Camarero, J., 2016. El registro sedimentario del lago Sant Maurici (Pirineos Centrales). Geogaceta 59, 11–14.

Carrillo, E., Ninot, J.M., 1998. Mapa De Vegetació De Catalunya a 1:50.000, Esterri D'Àneu 181. IEC-ICC. Barcelona.

Chmeleff, J., von Blanckenburg, F., Kossert, K., Jakob, D., 2010. Determination of the 10Be half-life by multicollector ICP-MS and liquid scintillation counting. Nucl. Instrum. Methods Phys. Res. B Beam Interact. Mater. Atoms 268, 192–199. https://doi.org/10.1016/j.nimb.2009.09.012.

Çiner, A., Oliva, M., Ventura, J., Akif Sarıkaya, M.A., Candas, A., David Palacios, D., Altınay, O., Steven, A., Binnie, S.A., Castaneda, N., 2024. Late Pleistocene glacial chronology and paleoclimate of the Cadí Massif, SE Pyrenees, Spain: insights from 36Cl cosmogenic surface exposure dating and glacier modelling. Quat. Sci. Rev. 345, 109020.

Copons, R., Bordonau, J., 1996. El registro sedimentario del Cuaternario reciente en el lago Redó d' Aigüestortes (Pirineos Centrales). In: Grandal d'Anglade, A., Pagés Valcarlos, J. (Eds.), IV Reunión De Geomorfología, pp. 249–258.

Crest, Y., Delmas, M., Braucher, R., Gunnell, Y., Calvet, M., Aster Team, 2017. Cirques have growth spurs during deglacial and interglacial periods: evidence from 10Be and 26Al nuclide inventories in the central and eastern Pyrenees. Geomorphology 278, 60–77. https://doi.org/10.1016/j.geomorph.2016.10.035.

Davies, B.J., 2022. Cryospheric Geomorphology: dating Glacial Landsforms II: radiometric techniques. In: Haritashya, U. (Ed.), Treatise on Geomorphology, vol. 4, pp. 249–280, 2.

Delmas, M., Gunnell, Y., Calvet, M., Reixach, T., Oliva, M., 2021. The pyrenees: glacial landforms from the last glacial maximum. In: Palacios, D., Hughes, P., García-Ruiz, J. M., Andrés, N. (Eds.), European Glacial Landscapes: Maximum Extent of Glaciations. Elsevier, pp. 461–472.

Delmas, M., Gunnell, Y., Calvet, M., Reixach, T., Oliva, M., 2023a. The pyrenees: environments and landforms in the aftermath of the LGM (18.9-14.6 ka) (chapter 21). In: Palacios, D., Hughes, P., García-Ruiz, J.M., Andrés, A. (Eds.), European Glacial Landscapes: the Last Deglaciation. Elsevier, pp. 185–200.

Delmas, M., Oliva, M., Gunnell, Y., Fernandes, M., Reixach, T., Fernández-Fernández, J. M., Calvet, M., 2023b. The Pyrenees: glacial landforms from the Bølling-Allerød Interstadial (14.6-12.9 ka) (chapter 38). In: Palacios, D., Hughes, P., García-Ruiz, J. M., Andrés, A. (Eds.), European Glacial Landscapes: the Last Deglaciation. Elsevier, pp. 361–368.

Delmas, M., Oliva, M., Gunnell, Y., Reixach, T., Fernandes, M., Fernández-Fernández, J. M., Calvet, M., 2023c. The Pyrenees: glacial landforms from the Younger Dryas (12.9-11.7 ka) (chapter 56). In: Palacios, D., Hughes, P., García-Ruiz, J.M., Andrés, A. (Eds.), European Glacial Landscapes: the Last Deglaciation. Elsevier, pp. 541–552.

Delmas, M., Oliva, M., Gunnell, Y., Fernández-Fernández, J.M., Reixach, T., Fernandes, M., Chapron, E., René, P., Calvet, M., 2024. The Pyrenees: glacial landforms from the Holocene (chapter 21). In: Palacios, D., Hughes, P., Jomelli, V., Tanarro, L.M. (Eds.), European Glacial Landscapes: the Holocene. Elsevier, pp. 419–439.

Dramis, F., Kotarba, A., 1994. Geomorphological evidences of high-mountain permafrost in central Apennnines. Geogr Fis Din Quat 17, 29–39.

Dunai, T.J., 2010. Cosmogenic Nuclides: Principles, Concepts and Application in the Earth Surface Sciences. Cambridge University Press, Cambridge. https://doi.org/10.1017/CBO9780511804519.

Dunne, J., Elmore, D., Muzikar, P., 1999. Scaling factors for the rates of production of cosmogenic nuclides for geometric shielding and attenuation at depth on sloped surfaces. Geomorphology 27, 3–11.

Fernandes, M., Oliva, M., Vieira, G., Palacios, D., Fernández- Fernández, J.M., García-Oteyza, J., Schimmelpfennig, I., Aster, Team, Antoniades, D., 2021. Glacial oscillations during the Bølling–Allerød Interstadial–Younger Dryas transition in the Ruda Valley, Central Pyrenees. J. Quat. Sci. 37, 42–58.

Fernandes, M., Oliva, M., Vieira, G., Lopes, L., 2022. Geomorphology of the Aran Valley (upper garonne Basin, central pyrenees). J. Maps 1–13. https://doi.org/10.1080/17445647.2022.2035266 (SCI IF: 2.7; Q1).

Fernandes, M., Oliva, M., Fernández-Fernández, J.M., Vieira, G., Palacios, D., García-Oteyza, J., Ventura, J., Schimmelpfenning, I., ASTER-Team, 2023. Geomorphological record of the glacial to periglacial transition from the Bølling–Allerød to the Holocene in the Central Pyrenees: the Locampo Cirque in the regional context. Boreas. https://doi.org/10.1111/bor.12633.ISSN0300-9483.

Fernández-Fernández, J.M., Palacios, D., García-Ruiz, J.M., Andrés, N., Schimmelpfennig, I., Gómez-Villar, A., Santos-González, J., Álvarez-Martínez, J., Arnáez, J., Úbeda, J., Léanni, L., ASTER Team, 2017. Chronological and geomorphological investigation of fossil debris-covered glaciers in relation to deglaciation processes: a case study in the Sierra de la Demanda, northern Spain. Quat. Sci. Rev. 170, 232–249.

Fontboté, J.M., Solé Sabarís, L., Alimen, H., 1957. Livret guide de l'excursion N1, Pyrénées. VI ème-VII ème journées. In: V Congreso Internacional INQUA. Madrid-Bacelona, pp. 65–74.

García-Ruiz, J.M., Palacios, D., González-Sampériz, P., de Andrés, N., Moreno, A., Valero-Garcés, B., Gómez-Villar, A., 2016. Mountain glacier evolution in the Iberian Peninsula during the Younger Dryas. Quat. Sci. Rev. 138, 16–30.

García-Ruiz, J.M., Palacios, D., Andrés, N., López-Moreno, J.I., 2020. Neoglaciation in the Spanish Pyrenees: a multiproxy challenge. Mediterranean Geoscience Reviews 2, 21–36.

García Sainz, L., 1935. Morfología glaciar y preglaciar de la región de la Noguera. Boletín la Soc. Geográfica Nacional 75, 64–130.

Giardino, J.R., Vitek, J.D., 1988. The significance of rock glaciers in the glacial-periglacial landscape continuum. Jour. Quat. Sci. 3, 97–103.

Giraudi, C., 2015. The Upper Pleistocene deglaciation on the Apennines (Peninsular Italy). Cuadernos de Investigación Geográfica 41 (2), 337–358.
Giraudi, C., Frezzotti, M., 1997. Late Pleistocene glacial events in the central apennines, Italy. Quaternary Research 48, 280–290.
Gosse, J.C., Phillips, F.M., 2001. Terrestrial in situ cosmogenic nuclides: theory and application. Quat. Sci. Rev. 20, 1475–1560.
Hamelin, L.E., 1958. Materiaux de geomorphologie periglaciaire dans l'Espagne du Nord. Rev. Geogr. Pyr. S-Ouest 5, 92–989.
Heyman, J., Stroeven, A.P., Harbor, J.M., Caffee, M.W., 2011. Too young or too old: evaluating cosmogenic exposure dating based on an analysis of compiled boulder exposure ages. Earth Planet Sci. Lett. 302, 71–80.
Hofmann, F.M., 2018. Glacial history of the Drac Blanc catchment (Écrins Massif, French Alps). Student Thesis Series INES, 459. Lund University, Sweden, p. 62.
Hughes, P.D., Allard, J.L., Woodward, C., Pope, J.J., 2023. The Balkans: glacial landforms during the Younger Dryas Stadial (chapter 59). In: Palacios, D., Hughes, P., García-Ruiz, J.M., Andrés, A. (Eds.), European Glacial Landscapes: the Last Deglaciation. Elsevier, pp. 571–579.
Institut Cartogràfic i Geològic de Catalunya, ICGC, 2007. Mapa Geològic Comarcal De Catalunya 1:50.000: Pallars Sobirà. Barcelona.
Ivy-Ochs, S., 2015. Glacier variations in the European Alps at the end of the last glaciation. Cuadernos de Investigación Geográfica 41 (2), 295–315.
Ivy-Ochs, S., Monegato, G., Reitner, J., 2023. The Alps: glacial landforms from the Younger Dryas Stadial (chapter 55). In: Palacios, D., Hughes, P., García-Ruiz, J.M., Andreś, A. (Eds.), European Glacial Landscapes: the Last Deglaciation. Elsevier, pp. 525–539.
Jomelli, V., Chapron, E., Favier, V., Rinterknecht, V., Braucher, R., Tournier, N., Gascoin, S., Marti, R., Galop, D., Binet, S., Deschamps, C., Tissoux, H., Aumaître, G., Bourlès, D.L., Keddadouche, K., 2020. Glacier fluctuations during the late glacial and Holocene on the Ariège Valley, northern slope of the Pyrenees and reconstructed climatic conditions. Mediterranean Geoscience Reviews 2, 37–51.
Kirkbride, M.P., Winkler, S., 2012. Correlation of late Quaternary moraines: impact of climate variability, glacier response, and chronological resolution. Quat. Sci. Rev. 46, 1–29.
Korschinek, G., Bergmaier, A., Faestermann, T., Gerstmann, U.C., Knie, K., Rugel, G., Wallner, A., Dillmann, I., Dollinger, G., von Gostomski, C.L., Kossert, K., Maiti, M., Poutivtsev, M., Remmert, A., 2010. A new value for the half-life of 10Be by heavy-ion elastic recoil detection and liquid scintillation counting. Nucl. Instrum. Methods Phys. Res. B Beam Interact. Mater. Atoms 268, 187–191. https://doi.org/10.1016/j.nimb.2009.09.020.
Lambiel, C., Maillard, B., Martin, S., Pellitero Ondicol, R., Schoeneich, P., Reynard, E., 2013. Adaptation of the geomorphological mapping system of the University of Lausanne for ArcGIS. In: 8th International Conference on Geomorphology (IAG), Paris, 27-31 Aug. 2013.
Lambiel, C., Maillard, B., Kummert, M., Reynard, E., 2016. Geomorphology of the Hérens Valley (Swiss Alps). J. Maps 12 (1), 160–172. https://doi.org/10.1080/17445647.2014.999135.
Lasberg, K., Kalm, V., 2013. Chronology of late Weichselian glaciation in the western part of the East European Plain. Boreas 42, 995–1007.
Leblanc, D., Gleizes, G., 1991. Estructura del massís de la Maladeta. La Investigació Al Parc Nacional D'Aigüestortes i Estany De Sant Maurici. II Jornades Sobre Recerca, pp. 11–21.
Lehmann, B., Anderson, R.S., Bodin, X., Cusicanqui, D., Valla, P.G., Carcaillet, J., 2022. Alpine rock glacier activity over Holocene to modern timescales (western French Alps). Earth Surf. Dynam. 10, 605–633.
Li, Y., 2018. Determining topographic shielding from digital elevation models for cosmogenic nuclide analysis: a GIS model for discrete sample sites. J. Mt. Sci. 15, 939–947.
Li, Y., 2023. Palaeolce: an automated method to reconstruct palaeoglaciers using geomorphic evidence and digital elevation models. Geomorphology 421 (July 2022), 108523. https://doi.org/10.1016/j.geomorph.2022.108523.
Lifton, N.A., Sato, T., Dunai, T.J., 2014. Scaling in situ cosmogenic nuclide production rates using analytical approximations to atmo- spheric cosmic-ray fluxes. Earth Planet Sci. Lett. 386, 149–160.
López-Moreno, J.I., Alonso-González, E., Monserrat, O., et al., 2018. Ground-based remote-sensing techniques for diagnosis of the current state and recent evolution of the Monte Perdido Glacier, Spanish pyrenees. J. Glaciol. 65, 85–100.
Makos, M., 2015. Deglaciation of the high Tatra Mountains. Cuadernos de Investigación Geográfica 41 (2), 317–335.
Martí-Bono, C., Puigdefàbregas, C., 1968. Estudio del Parque Nacional de Aigües Tortes y Lago San Mauricio: geología y geomorfología. Centro Pirenaico de Biología Experimental 2, 7–37.
Martin, L.C.P., Blard, P.H., Balco, G., Lavé, J., Delunel, R., Lifton, N.A., Laurent, V., 2017. The CREp program and the ICE-D production rate calibration database: a fully parameterizable and updated online tool to compute cosmic-ray exposure ages. Quat. Geochronol. 38, 25–49.
Merchel, S., Herpers, U., 1999. An update on radiochemical separation techniques for the determination of long-lived radio- nuclides via accelerator mass spectrometry. Radiochim. Acta 84, 215–219.
Merchel, S., Arnold, M., Aumaître, G., et al., 2008. Nuclear Instruments and Methods in Physics Research B Towards more precise 10 Be and 36 Cl data from measurements at the 10 À 14 level: influence of sample preparation Be/B e. Nucl. Instrum. Methods Phys. Res. Sect. B Beam Interact. Mater. Atoms 266, 4921–4926.
Moran, A.P., Ivy-Ochs, S., Vockenhuber, C., Kerschner, H., 2016a. Rock glacier development in the Northern Calcareous Alps at the Pleistocene-Holocene boundary. Geomorphology 273, 178–188.
Moran, A.P., Ivy-Ochs, S., Vockenhuber, C., Kerschner, H., 2016b. First 36Cl exposure ages from a moraine in the Northern Calcareous Alps. Quaternary Science Journal 65 (2), 145–155.
Muñoz, J.A., 1992. Evolution of a continental collision belt: ecors-pyrenees crustal balanced cross-section, dins de. In: MCCLAY, K.R. (Ed.), Thrust Tectonics. Springer-Science, London, pp. 235–246.
Naughton, F., Toucanne, S., Landais, A., Rodrigues, T., Vazquez Riveiros, N., María, F., Sánchez-Goñi, M.F., 2023a. Heinrich Stadial 1 (chapter 5). In: Palacios, D., Hughes, P., García-Ruiz, J.M., Andrés, A. (Eds.), European Glacial Landscapes: the Last Deglaciation. Elsevier, pp. 37–44.
Naughton, F., Sánchez-Goñi, M.F., Landais, A., Rodrigues, T., Vazquez Riveiros, N., Toucanne, S., 2023b. The Bølling-Allerød Interstadial (chapter 6). In: Palacios, D., Hughes, P., García-Ruiz, J.M., Andrés, A. (Eds.), European Glacial Landscapes: the Last Deglaciation. Elsevier, pp. 45–50.
Naughton, F., Sánchez-Goñi, M.F., Landais, A., Rodrigues, T., Vazquez Riveiros, N., Toucanne, S., 2023c. The Younger Dryas stadial (chapter 7). In: Palacios, D., Hughes, P., García-Ruiz, J.M., Andrés, A. (Eds.), European Glacial Landscapes: the Last Deglaciation. Elsevier, pp. 51–55.
Nussbaum, F., 1934. Die See der Pyrenäen. Mitt der Naturforsch. Ges., 184
Nussbaum, F., 1956. Observations morphologiques dans la région de la Noguera Pallaresa. Pirineos 39, 57–95.
Oliva, M., Palacios, D., Fernández-Fernández, J.M., Rodríguez-Rodríguez, L., García-Ruíz, J.M., Andrés, N., Carrasco, R.M., Pedraza, J., Pérez-Alberti, A., Valcárcel, M., Hughes, P.D., 2019. Late Quaternary glacial phases in the Iberian Peninsula. Earth Sci. Rev. 192, 564–600.
Oliva, M., Fernandes, M., Palacios, D., Fernández-Fernández, J.M., Schimmelpfennig, I., , ASTER Team, Antoniades, D., 2021. Rapid deglaciation during the Bølling-Allerød interstadial in the Central Pyrenees and associated glacial and periglacial landforms. Geomorphology 385, 107735. https://doi.org/10.1016/j.geomorph.2021.107735.
Oliva, M., Palacios, D., Fernández-Fernández, J.M. (Eds.), 2022. Iberia, Land of Glaciers: How the Mountains were Shaped by Glaciers. Elsevier, Amsterdam, p. 618.
Oliva, M., Andrés, N., Fernández-Fernández, Palacios, D., 2023. The evolution of glacial landforms in the Iberian Mountains during the Younger Dryas Stadial (chapter 57). In: Palacios, D., Hughes, P., García-Ruiz, J.M., Andrés, A. (Eds.), European Glacial Landscapes: the Last Deglaciation. Elsevier, pp. 553–562.
Palacios, D., Andrés, N., Marcos, J., Vázquez-Selem, L., 2012a. Glacial máximum advance and deglaciation of the Pinar Valley (Sierra de Gredos, Central Spain) and its significance in the Mediterranean context. Geomorphology 177–178, 51–61. https://doi.org/10.1016/j.geomorph.2012.07.013.
Palacios, D., de Andrés, N., de Marcos, J., Vázquez-Selem, L., 2012b. Glacial landforms and their paleoclimatic significance in Sierra de Guadarrama, central Iberian peninsula. Geomorphology 139, 67–78.
Palacios, D., de Andrés, N., López-Moreno, J.I., García-Ruíz, J.M., 2015. Late Pleistocene deglaciation in the upper Gállego Valley, central Pyrenees. Quaternary Research. https://doi.org/10.1016/j.yqres.2015.01.010, 2015.
Palacios, D., Gómez-Ortiz, A., Andrés, N., Salvador, F., Oliva, M., 2016. Timing and new geomorphological evidence of the last deglaciation stages in Sierra Nevada (southern Spain). Quat. Sci. Rev. 150, 110–129. https://doi.org/10.1016/jquascirev.2016.08.012.
Palacios, D., García-Ruíz, J.M., de Andrés, N., Schimmelpfennig, I., Campos, N., Léanni, L., ASTER Team, 2017. Deglaciation in the central Pyrenees during the Pleistocene-Holocene transition: timing and geomorphological significance. Quat. Sci. Rev. 162, 111–127.
Palacios, D., Oliva, M., Gómez-Ortiz, A., Andrés, N., José, M., Fernández-Fernández, J. M., Schimmelpfennig, I., Léanni, L., Team, A.S.T.E.R., 2020. Climate sensitivity and geomorphological response of cirque glaciers from the late glacial to the Holocene, Sierra Nevada, Spain. Quat. Sci. Rev. 248 (2). https://doi.org/10.1016/j.quascirev.2020.106617.
Palacios, D., Hughes, D., García-Ruiz, J.M., Andrés, N., 2023. The importance of European glacial landscape in a context of great climatic variability (chapter 62). In: Palacios, D., Hughes, P., García-Ruiz, J.M., Andrés, A. (Eds.), European Glacial Landscapes: the Last Deglaciation. Elsevier, pp. 605–617.
Pallàs, R., Rodés, A., Braucher, R., Carcaillet, J., Ortuño, M., Bordonau, J., Bourlès, D., Vilaplana, J.M., Masana, E., Santanach, P., 2006. Late Pleistocene and Holocene glaciation in the Pyrenees: a critical review and new evidence from 10Be exposure ages, South-Central Pyrenees. Quat. Sci. Rev. 25, 2937e2963. https://doi.org/10.1016/j.quascirev.2006.04.004.
Pellitero, R., 2014. Geomorphology and geomorphological landscapes of Fuentes Carrionas. J. Maps 10 (2), 313–323. https://doi.org/10.1080/17445647.2013.867822.
Porter, S.C., 1975. Equilibrium-line altitudes of late Quaternary glaciers in the Southern Alps, New Zealand. Quaternary Research 5 (1), 27–47. https://doi.org/10.1016/0033-5894(75)90047-2.
Pyrda, A., 2023. Glacial geomorphology and Pleistocene glacier reconstruction in the Demänovská Valley, low Tatra Mountains, Slovakia. Geology, Geophysics & Environment 49 (1), 19–36.
Rasmussen, S.O., Bigler, M., Blockley, S.P., Blunier, T., Buchardt, S.L., Clausen, H.B., Cvijanovic, I., Dahl-Jensen, D., Johnsen, S., Fischer, H., Gkinis, V., Guillevic, M., Hoek, W.Z., Lowe, J., Pedro, J.B., Popp, T., Seierstad, I.K., Steffensen, J.P., Svensson, A.M., Vallelonga, P., Vinther, B.M., Walker, M., Wheatley, J.J., Winstrup, M., 2014. A stratigraphic framework for abrupt climatic changes during the last glacial period based on three synchronized Greenland ice-core records: refining and extending the INTIMATE event stratigraphy. Quat. Sci. Rev. 106, 14–28.
Rea, B.R., 2009. Defining modern day Area-Altitude Balance Ratios (AABRs) and their use in glacier-climate reconstructions. Quat. Sci. Rev. 28 (3–4), 237–248. https://doi.org/10.1016/j.quascirev.2008.10.011.

Rea, B.R., Pellitero, R., Spagnolo, M., Hughes, P., Ivy-Ochs, S., Renssen, H., Ribolini, A., Bakke, J., Lukas, S., Braithwaite, R.J., 2020. Atmospheric circulation over Europe during the Younger Dryas. Sci. Adv. 6. https://doi.org/10.1126/sciadv.aba4844 eaba4844.

René, P., 2011. Régression des glaciers pyrénéens et transformation du paysage depuis le Petit Âge Glaciaire. Sud-Ouest Eur. 32, 5–19.

RGIK, 2023. Guidelines for inventorying rock glaciers: baseline and practical concepts (version 1.0). IPA Action Group Rock Glaciers Inventories and Kinematics, p. 25. https://doi.org/10.51363/unifr.srr.2023.002.

Ribolini, A., Chelli, A., Guglielmin, M., Pappalardo, M., 2007. Relationships betwenn glaciar and rock glacier in the Maritime Alps, Schiantala Valley, Italy. Quaternary Research 68, 353–363.

Ribolini, A., Spagnolo, M., Giraudi, C., 2023. The Italian Mountains: glacial landforms from the Younger Dryas Stadial (12.9-11.7 ka) (chapter 58). In: Palacios, D., Hughes, P., García-Ruiz, J.M., Andreś, A. (Eds.), European Glacial Landscapes: the Last Deglaciation. Elsevier, pp. 563–570.

Rodríguez-Rodríguez, L., Domínguez-Cuesta, M.J., Rinterknecht, V., Jiménez-Sánchez, M., González-Lemos, S., Leanni, L., Jorge Sanjurjo, J., Ballesteros, D., Valenzuela, P., Llana-Fúnez, S., ASTER Team, 2017. Constraining the age of superimposed glacial records in mountain environments with multiple dating methods (Cantabrian Mountains, Iberian Peninsula). Quat. Sci. Rev. 195, 215–231.

Rull, V., Blasco, A., Calero, M.A., Blaauw, M., Vegas-Vilarrúbia, T., 2023. A continuous Centennial late glacial-early Holocene (15–10 cal kyr BP) palynological record from the Iberian pyrenees and regional comparisons. Plants 12 (20), 3644. https://doi.org/10.3390/plants12203644.

Ruszkiczay-Rüdiger, Z., Kern, Z., Urdea, P., Braucher, R., Madarász, B., Schimmelpfennig, I., 2016. Revised deglaciation history of the Pietrele Stânisoara glacial complex, Retezat Mts, Southern Carpathians, Romania. Quat. Int. 415, 216–229. https://doi.org/10.1016/j.quaint.2015.10.085.

Sarıkaya, M.A., Zreda, M., Ciner, A., 2009. Glaciations and paleoclimate of Mount Erciyes, central Turkey, since the Last Glacial Maximum, inferred from 36Cl cosmogenic dating and glacier modeling. Quat. Sci. Rev. 28 (23–24), 2326–2341. https://doi.org/10.1016/j.quascirev.2009.04.015.

Schoeneich, P., 1993. Comparaison des systèmes de légende français, allemand et suisse. In: Schoeneich, P., Reynard, E. (Eds.), Cartographie Géomorphologique - Cartographie Des Risques. Actes De La Réunion Annuelle De La Société Suisse De Géomorphologie, 19 Au 21 Juin 1992 Aux Diablerets Et À Randa. Institut de Géographie Lausanne, Lausanne, pp. 15–24.

Serrat, D., Bordonau, J., Bru, J., Furdada, G., Gomez, A., Marti, J., Martí, M., Salvador, F., Ventura, J., Vilaplana, J.M., 1994. Síntesis cartográfica del glaciarismo surpirenaico oriental. In: Bono, C.M., García-Ruiz, J.M. (Eds.), El Glaciarismo Surpirenaico: Nuevas Aportaciones. Geoforma, Logroño, pp. 9–15.

Solé i Sabarís, L., 1936. Els Llacs dels Pirineus, segons Nussbaum. Butlletí de la Inst. Catalana d' Història Natural 36, 107–115.

Solomina, O.N., Bradley, R.S., Hodgson, D.A., et al., 2015. Holocene glacier fluctuations. Quat. Sci. Rev. 111, 9–34. https://doi.org/10.1016/j.quascirev.2014.11.018.

Steinemann, O., Reitner, J.M., Ivy-Ochs, S., Christl, M., Synal, H.A., 2020. Tracking rock-glacier evolution in the Eastern Alps from the Lateglacial to the early Holocene. Quat. Sci. Rev. 241, 106424.

Taillefer, F., 1957. Glaciaire Pyrénnéen: versant Nord et versant Sud. Rev. Geogr. Pyr. S-Ouest 28, 221–224.

Tomkins, M.D., Dortch, J.M., Hughes, P.D., Huck, J.J., Stimson, A.G., Delmas, M., Calvet, M., Pallàs, R., 2018. Rapid age assessment of glacial landforms in the Pyrenees using Schmidt hammer exposure dating (SHED). Quaternary Research 90 (1), 26–37. https://doi.org/10.1017/qua.2018.12.

Turu, V., Peña-Monné, J.L., Cunha, P.P., Jalut, G., Buylaert, J.P., Murray, A.S., Bridgland, D., Faurschou-Knudsen, M., Oliva, M., Carrasco, R., Ros, X., Turu-Font, L., Ventura, J., 2023. Glacial–interglacial cycles in the south-central and southeastern Pyrenees since ~180 ka (NE Spain–Andorra–S France). Quaternary Research 1–28. https://doi.org/10.1017/qua.2022.68, 2023.

Urdea, P., Ardelean, F., Ardelean, M., Onaca, A., 2023. The Romanian carpathians: glacial landforms during Bølling Allerød Interstadial (14.6-12.9 ka). In: Palacios, D., Hughes, P., García-Ruiz, J.M., Andrés, A. (Eds.), European Glacial Landscapes: the Last Deglaciation. Elsevier, pp. 347–353.

Urdea, P., Ardelean, F., Ardelean, M., Onaca, A., Berzescu, O., 2024. Glacial landscape evolution during the Holocene in the Romanian Carpathians. In: Palacios, D., Hughes, P., Jomelli, V., Tanarro, L.M. (Eds.), European Glacial Landscapes: the Holocene. Elsevier, pp. 331–351.

Urdea, P., Ardelean, F., Ardelean, M., Onaca, A., Berzescu, O., 2023. The Romanian carpathians: glacial landforms from the Younger Dryas (chapter 54). In: Palacios, D., Hughes, P., García-Ruiz, J.M., Andrés, A. (Eds.), European Glacial Landscapes: the Last Deglaciation. Elsevier, pp. 517–524.

Uppala, S.M., 2005. The ERA-40 re-analysis. Q. J. R. Meteorol. Soc. 131, 2961–3012.

Ventura, J., 1983. Geomorfologia Glacial De La Vall D'Espot (Palars Sobirà, Pirineu Central). Universitat de Barcelona. Tesis de Llicenciatura, p. 231.

Ventura, J., 2017. Identificación de fases glaciares durante la deglaciación en el Macizo de Monteixo-Medacorba (Pirineo Central, Lleida). En. In: Ruíz-Fernández, J., García-Hernández, C., Oliva, M., Rodríguez-Pérez, C., Gallinar, D. (Eds.), Ambientes Periglaciares: Avances En Su Estudio, Valoración Patrimonial Y Riesgos Asociados. Servicio de Publicaciones de la Universidad de Oviedo, pp. 137–146.

Ventura, J., 2020. Distribución espacial y temporal de glaciares, glaciares cubiertos y glaciares rocosos durante la última deglaciación en el valle de la Bonaigua (Pirineo Central). Cuadernos de investigación geográfica 46 (2), 413–446.

Ventura, J., Turu, V., 2022. The glaciers of the Central-Eastern Pyrenees. In: Oliva, M., Palacios, D., Fernández-Fernández, J.M. (Eds.), Iberia, Land of Glaciers. Elsevier, Amsterdam, pp. 87–121.

Vidaller, I., 2025. Past, Present and Future of the Ésera Glacier. Paleoenvironmental Evolution and Recent Deglaciation. University of Zaragoza, p. 397. Ph D Thesis.

Walker, M., Head, M.J., Berkelhammer, M., Björck, S., Hai Cheng, H., Cwynar, L., Fisher, D., Gkinis, V., Long, A., Lowe, J., Newnham, R., Rasmussen, S.O., Weiss, H., 2018. Formal ratification of the subdivision of the Holocene Series/Epoch (Quaternary System/Period): two new Global Boundary Stratotype Sections and points (GSSPs) and three new stages/subseries. Episodes 41 (4), 213–223. https://doi.org/10.18814/epiiugs/2018/018016.

Ward, G.K., Wilson, S.R., 1978. Procedures for comparing and combining radiocarbon age determination: a critique. Archaeometry 20, 19–31. https://doi.org/10.1111/j.1475-4754.1978.tb00208.x.

Yeşilyurt, S., 2025. The role of Little Ice Age glaciation in shaping the rock glacier morphology of Mount Kaçkar, Türkiye. Mediterranean Geoscience Reviews. https://doi.org/10.1007/s42990-025-00160-y.

Zandvliet, J., 1960. The geology of the upper Salat and Pallaresa valleys, Central Pyrenees, France/Spain. Leidse Geol. Meded. 25, 1–127.

Zasadni, J., Kłapyta, P., 2016. From valley to marginal glaciation in alpine-type relief: lateglacial glacier advances in the Piéc Stawów Polskich/Roztoka Valley, high Tatra Mountains, Poland. Geomorphology 253, 406–424. https://doi.org/10.1016/j.geomorph.2015.10.032.

Zasadni, J., Klapyta, P., Brós, E., Ivy-Ochs, S., Swiader, A., Christl, M., Balázovicová, L., 2020. Latest Pleistocene glacier advances and post-younger Dryas rock glacier stabilization in the mt. Kriváň group, high Tatra Mountains, Slovakia. Geomorphology 358, 107093.

Zasadni, J., Klapyta, P., Toloczko-Pasek, A., Makos, M., 2023a. The evolution of glacial landforms un the Tatra Mountains during the Younger Dryas (chapter 53). In: Palacios, D., Hughes, P., García-Ruiz, J.M., Andrés, A. (Eds.), European Glacial Landscapes: the Last Deglaciation. Elsevier, pp. 509–515.

Zasadni, J., Klapyta, P., Makos, M., 2023b. The evolution of glacial landforms in the Tatra Mountains during the deglaciation. In: Palacios, D., Hughes, P., García-Ruiz, J. M., Andrés, A. (Eds.), European Glacial Landscapes: the Last Deglaciation. Elsevier, pp. 157–164.